NASA/TP-2016-219220

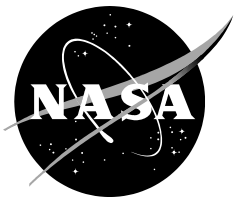

Development of Detonation Modeling Capabilities for Rocket Test Facilities: Hydrogen-Oxygen-Nitrogen Mixtures

Daniel C. Allgood
Stennis Space Center, Mississippi

April 2016

NASA STI Program ... in Profile

Since its founding, NASA has been dedicated to the advancement of aeronautics and space science. The NASA scientific and technical information (STI) program plays a key part in helping NASA maintain this important role.

The NASA STI program operates under the auspices of the Agency Chief Information Officer. It collects, organizes, provides for archiving, and disseminates NASA's STI. The NASA STI program provides access to the NTRS Registered and its public interface, the NASA Technical Reports Server, thus providing one of the largest collections of aeronautical and space science STI in the world. Results are published in both non-NASA channels and by NASA in the NASA STI Report Series, which includes the following report types:

- TECHNICAL PUBLICATION. Reports of completed research or a major significant phase of research that present the results of NASA Programs and include extensive data or theoretical analysis. Includes compilations of significant scientific and technical data and information deemed to be of continuing reference value. NASA counter-part of peer-reviewed formal professional papers but has less stringent limitations on manuscript length and extent of graphic presentations.

- TECHNICAL MEMORANDUM. Scientific and technical findings that are preliminary or of specialized interest, e.g., quick release reports, working papers, and bibliographies that contain minimal annotation. Does not contain extensive analysis.

- CONTRACTOR REPORT. Scientific and technical findings by NASA-sponsored contractors and grantees.

- CONFERENCE PUBLICATION. Collected papers from scientific and technical conferences, symposia, seminars, or other meetings sponsored or co-sponsored by NASA.

- SPECIAL PUBLICATION. Scientific, technical, or historical information from NASA programs, projects, and missions, often concerned with subjects having substantial public interest.

- TECHNICAL TRANSLATION. English-language translations of foreign scientific and technical material pertinent to NASA's mission.

Specialized services also include organizing and publishing research results, distributing specialized research announcements and feeds, providing information desk and personal search support, and enabling data exchange services.

For more information about the NASA STI program, see the following:

- Access the NASA STI program home page at http://www.sti.nasa.gov

- E-mail your question to help@sti.nasa.gov

- Phone the NASA STI Information Desk at 757-864-9658

- Write to:
  NASA STI Information Desk
  Mail Stop 148
  NASA Langley Research Center
  Hampton, VA 23681-2199

NASA/TP-2016-219220

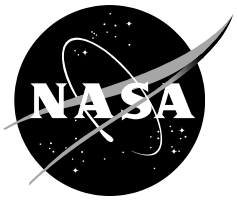

Development of Detonation Modeling Capabilities for Rocket Test Facilities: Hydrogen-Oxygen-Nitrogen Mixtures

Daniel C. Allgood
Stennis Space Center, Mississippi

National Aeronautics and
Space Administration

Stennis Space Center
Stennis Space Center, MS 39529-6000

April 2016

Acknowledgments

The author would like to thank the following technical reviewers for their valuable contributions to this document: Daniel Jones (NASA-SSC), Harry Ryan (NASA-SSC), and Brandon Williams (CFD Research Corporation/NASA-MSFC).

Development of Detonation Modeling Capabilities for Rocket Test Facilities: Hydrogen-Oxygen-Nitrogen Mixtures

Daniel C. Allgood
Engineering and Test Directorate, Design and Analysis Division
NASA Stennis Space Center, MS 39529-6000

The objective of the presented work was to develop validated computational fluid dynamics (CFD) based methodologies for predicting propellant detonations and their associated blast environments. Applications of interest were scenarios relevant to rocket propulsion test and launch facilities. All model development was conducted within the framework of the Loci/CHEM CFD tool due to its reliability and robustness in predicting high-speed combusting flow-fields associated with rocket engines and plumes. During the course of the project, verification and validation studies were completed for hydrogen-fueled detonation phenomena such as shock-induced combustion, confined detonation waves, vapor cloud explosions, and deflagration-to-detonation transition (DDT) processes. The DDT validation cases included predicting flame acceleration mechanisms associated with turbulent flame-jets and flow-obstacles. Excellent comparison between test data and model predictions were observed. The proposed CFD methodology was then successfully applied to model a detonation event that occurred during liquid oxygen/gaseous hydrogen rocket diffuser testing at NASA Stennis Space Center.

Nomenclature

AFRL	= Air Force Research Laboratory
BR	= area blockage ratio
CEA	= Chemical Equilibrium Analysis Code
CFD	= computational fluid dynamics
CJ	= Chapman Jouguet condition
d	= orifice diameter
D	= jet or pipe diameter
DDT	= deflagration-to-detonation transition
DL	= Darrieus-Landau instability
dx, dy, dz	= mesh or grid spacing
E_o	= energy released by the propellant detonation
GH2	= gaseous hydrogen
GO2	= gaseous oxygen
H2	= hydrogen
HBMS	= Hirschfelder-Buehler-McGee- Sutton
HLLE	= Hessian Locally Linear Embedding
HUCTA	= Hydrogen Unconfined Combustion Test Apparatus
L_{ind}	= induction length
LH2	= liquid hydrogen
LO2	= liquid oxygen
M	= Mach number
MPTA	= Main Propulsion Test Article
N2	= nitrogen
NASP	= National Aerospace Plane
O2	= oxygen

P	= pressure
P_o	= initial pressure of the propellant
PL	= power level
r	= reactions or fluid density
s	= species
SRK	= Soave-Redlich-Kwong
SSC	= Stennis Space Center
stoich	= stoichiometric condition
STP	= standard-state temperature and pressure (298 K, 1 atm)
t	= time
T	= temperature
TNT	= trinitrotoluene
U	= wave speed
V	= velocity
V_o	= initial volume of the propellant
VCE	= vapor cloud explosion
VN	= von-Neumann condition
W	= weight of propellant
x, y, z	= Cartesian coordinates
Y	= mass fraction
β	= molar ratio of nitrogen to oxygen
Φ	= equivalence ratio
λ	= detonation cell width
ρ	= density
θ	= directivity angle relative to rocket diffuser exit

I. Introduction

NASA Stennis Space Center (SSC) was originally established for conducting liquid rocket propulsion testing in support of NASA space exploration programs. Over the years, SSC has expanded its rocket propulsion test services to include both Department of Defense and commercial space launch customers. As part of this ongoing role of rocket propulsion testing, SSC has been supporting research and development test programs for smaller scale thrusters, turbo-pumps and other various rocket engine systems.

One of the principal concerns regarding concurrent testing of multiple engines is the potential for a propellant detonation to occur. Testing of chemical rocket propulsion systems involves the potential for high-energy explosions due to external release and/or delayed ignition of propellant flows. Figure 1 provides two examples where liquid H2-O2 engines ignited externally to the engine and large semi-spherical deflagration flame fronts were generated. In both cases, the ignition was a result of external safety-ignition devices designed to minimize the overpressure created by such events. The ability to predict these blast environments is critical to the safety of the test/launch facility as they can generate strong overpressure waves with the potential to damage the test article or flight hardware installed in a neighboring test cell. The Design and Analysis Division at SSC determined that there was a critical lack of knowledge, tools and understanding for reliably predicting the blast-wave environments a propellant detonation event would generate during a maximum credible failure. This is partially due to the complex facility structure present around the various test articles preventing a direct analytical prediction of the blast propagation and reflections that might occur. Thus, there was a need for the NASA community to develop a reliable and consistent methodology for modeling the source

of the detonation event and associated blast wave physics using high-fidelity computational fluid dynamics (CFD) tools.

In 2012, at the request of SSC, the NASA Engineering Safety Center (NESC) established a team of engineers from various NASA, Army and contractor facilities to examine the problem and develop tools and techniques for predicting blast-wave environments from rocket engine propellant detonations [1]. The objective was to provide reliable estimates of the dynamic loading experienced by test hardware in one test cell given a credible failure in a neighboring test cell. Using this predictive capability, SSC and the propulsion test customer could then make an informed decision as to whether mitigation or protection of the test articles was required. Due to time constraints, the NESC investigation focused on CFD-based methodologies for simulating blast wave propagations through large complex structures by assuming the source originated from an equivalent high-density explosive (e.g. TNT or C-4). The investigation was successful in validating and developing best practices for modeling blast dynamics in large domains of interest under these scenarios, and the work was presented at a special session of the 60th JANNAF Joint Propulsion Meeting. However, a key recommendation at the conclusion of the NESC investigation was to continue the work by extending the CFD predictive tool to the source of the propellant detonation rather than “equating” it to an assumed percent-yield of TNT. Also, it was deemed crucial not only to demonstrate the capability of predicting the detonation wave structure and dynamics, but also demonstrate the feasibility of predicting whether or not a detonation would even occur. Therefore, the current project was established with the goal of systematically demonstrating a valid engineering-level approach for predicting cryo-vapor cloud detonations (VCD), which are the primary source of blast wave events of concern on rocket test stands.

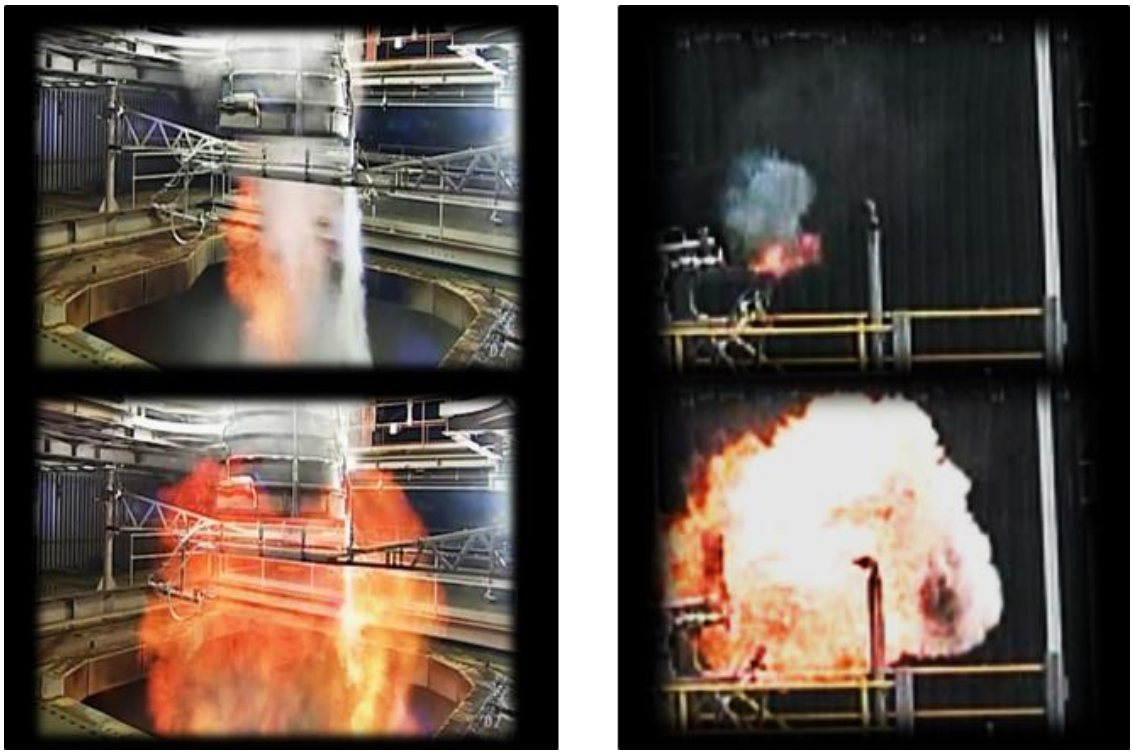

(a) **(b)**

Figure 1: External Ignition Events During LO2-LH2 Rocket Engine Testing at the SSC (a) A-1 and (b) E-1 Test Stands

II. Project Tasks

Table 1 summarizes each of the four tasks and associated sub-tasks pursued during this study. The first was a developmental task to understand the fundamental efficacy of simplified reaction mechanisms for H2-O2-N2 detonations prior to investigating any realistic rocket propellant detonation scenarios. Since most applications of liquid rocket propellant detonations involve hydrogen, oxygen and some amount of nitrogen dilution from the air, the selection of a well-documented validation test case involving H2-Air was desired. Ultimately, a steady shock-induced combustion scenario was selected for evaluating a series of reduced chemical mechanisms. The steady detonation wave allowed for quick simulations to gauge the performance of the code and reaction mechanisms on predicting detonation wave structure (e.g. shock standoff distance and combustion induction lengths) and ascertain sensitivities to mesh requirements and solver settings. The development task also provided a means of down-selecting to one or two sets of mechanisms to be used in the follow-on tasks.

Table 1: Project Task Summary

1. Developmental Task: Selection of Reduced-Chemical Mechanisms

- *Steady Axisymmetric Detonation:* Shock-Induced Combustion of H2-Air @ M=6.46 (Lehr)

2. Verification Tasks: Detonation Wave Propagation

- *Planar Detonation:* Stoichiometric H2-Air Detonation CJ Properties (NASA CEA)
- *Vapor Cloud Explosions (VCE):* CFD vs. TNT Equivalency, Analytical & Test Data

3. Validation Tasks: Deflagration-to-Detonation Transition (DDT)

- *Axisymmetric DDT with Obstacles:* Chapin & Lee H2-Air Orifices
- *3D DDT with Obstacles:* AFRL H2-Air Shchelkin-Type Spiral
- *Flame-Jet Initiation (Direct & DDT):* CALTECH HYJET H2-O2-N2 Jet Initiation Studies

4. Application to Rocket Propulsion Testing

- *LO2-GH2 Altitude Rocket Diffuser Detonation Event at SSC E-3 Facility*

Once the developmental task was completed, two verification tasks were identified to further confirm the CFD code's ability to predict the basic structure of H2-O2-N2 detonations. First, planar detonation wave modeling was performed to verify the correct Chapman-Jouguet (CJ) conditions were being computed at stoichiometric and non-stoichiometric conditions, and to further down select to a final chemical mechanism. Second, spherical vapor cloud explosion modeling would provide a means to ascertain mesh requirements and solver settings to maintain robust and accurate modeling of detonation source events and blast wave propagations. Also, since VCE is relevant to rocket propulsion testing, current engineering approaches (such as TNT equivalency curves) could be compared to the CFD-based approach being proposed.

Validation of the CFD modeling tool in predicting detonation events was best achieved by modeling several controlled deflagration-to-detonation transition (DDT) configurations reported in literature. The first validation task was to simulate an axisymmetric DDT event that utilized a series of orifice plates. Successful completion of this validation scenario would then follow with a

geometrical configuration, such as the Shchelkin-type spiral, that involved a strong three-dimensional flow behavior. By modeling a three-dimensional DDT process, the CFD tool would be challenged in both mesh size and computational time. The final validation test case identified was one of more direct application to rocket propulsion testing. It was deemed advantageous to assess the ability in predicting unconfined DDT of H2-O2-N2 mixtures via turbulent flame-jets, as this is the basic configuration utilized at rocket test facilities. Typically, a H2-O2 torch is used to inject a high-speed flame-jet into the exhaust of the rocket engine near the nozzle exit plane. This is done to ignite any excess hydrogen that did not burn by the combustor and thereby prevent a detonation or limit the amplitude of overpressure generated by a high-speed deflagration.

III. Loci/CHEM CFD Code Description

The Loci/CHEM code [2,3,4] is being developed at Mississippi State University partly under the sponsorship of NASA. CHEM utilizes the Loci numerical framework [5,6] to simulate three-dimensional turbulent, chemically reacting, compressible flows in a density-based finite-volume CFD program. Loci is a rule-based approach for implementing and directing the communication among the various numerical methods being used in the simulation. CHEM is a second-order accurate (time and space), density-based flow solver with capabilities such as turbulence modeling, adaptive meshing, finite-rate chemistry, and real-fluid equations of state and Lagrangian particle modeling for two-phase flows. CHEM has been designed to utilize distributed memory systems for parallel computing with the capability of automatic dynamic partitioning. This is highly advantageous as it eliminates the need for a user pre-processing setup, allowing for rapid reconfiguration to a different number of processors should hardware availability dictate such a change. A detailed documentation of the governing equation formulation and numerical approaches may be found in the Loci/CHEM user's manual [7]. Some of the key features have been summarized below.

Loci/CHEM implements a three-dimensional, finite-volume procedure in the discretization of the Navier-Stokes and supporting equations for generalized unstructured meshes. Since the solver is built on a cell-centered approach, any arbitrary polyhedral cell can be used in the calculations, including hanging nodes that are used in adaptive mesh refinement techniques. High-resolution approximate Riemann solvers are employed to enable a total variation diminishing solution. Two common inviscid flux limiters (Barth and Venkatakrishnan) are available to prevent spurious fluctuations in the Roe scheme. In addition to the Roe scheme, the HLLE approximate Riemann solver is available to correct carbuncle issues which frequently arise around strong Mach disks in rocket exhaust plumes. Time integration is available using the 2^{nd} order implicit Beam and Warming routine, or a local time stepping approach can be used to reach steady-state simulation results.

In the density-based formulation of Loci/CHEM, pressure is computed using Dalton's Law for a mixture of calorically imperfect (or thermally perfect) gases. In addition to the perfect gas equation of state, Loci/CHEM also has the capability of modeling real-fluid behavior via the SRK, Peng-Robinson, or HBMS equations of state. The Jones-Wilkins-Lee (JWL) equation of state is also available for high-density explosive detonation products. Temperature dependent specific heats can be modeled using the JANAF database [8], while viscosity and thermal diffusivity for each species can be modeled using Sutherland's Law or temperature-dependent database curve fits. Lastly, finite-rate chemical reactions of the species are modeled using customizable Arrhenius-type reaction sets.

Recent experience with the Loci/CHEM code led the author to its selection in the current study. It has also been routinely used by other NASA engineers for a variety of rocket modeling

applications such as liquid rocket nozzle film cooling [9] and launch pad environments [10]. In the current modeling efforts, the following solver conditions were common to all models. First, the participating species were assumed to be mixtures of calorically imperfect gases, where both transport and diffusion properties were temperature dependent. In addition, turbulence was modeled using Menter's Baseline (BSL) model [11]. The BSL model is a blended k-epsilon/k-omega model, and was combined with Wilcox's compressibility corrections to provide improved predictions for high speed flow applications.

IV. Evaluation of Reduced-Chemical Mechanisms using Shock-Induced H2-Air Combustion

A. Background

Prior to investigating specific applications directly related to rocket engine testing, the efficacy of simplified reaction mechanisms in representing H2-O2-N2 detonations within the Loci/CHEM framework needed to be understood. Since numerous chemical mechanisms ranging from very simplified global-type reactions to more elaborate mechanisms were initially of interest, selection of a validation test case that exhibited a steady-state detonation wave structure was advantageous. This minimized both the domain size and time-integration requirements for simulating a transient detonation propagation problem. In addition, validation using a steady detonation wave allowed quick assessments of mesh resolution requirements and numerical techniques. While numerous fundamental studies have been conducted in the past to achieve this goal, evaluation and proper down-selection of various chemical mechanisms specifically within the Loci/CHEM CFD framework was a critical step in the process of gaining confidence in the code's ability to model detonation-related phenomena.

In 1972, Lehr [12] published an experimental study of stoichiometric H2-Air, shock-induced combustion over a 15 mm diameter, spherical nose projectile. Lehr's shadowgraphs, shown in Figure 2, depict combustion modes exhibited under various H2-Air mixture velocities. The critical parameter varied was the ratio of flow velocity to the theoretical CJ detonation wave speed. For example, steady-state detonation conditions were generated when the mixture velocity exceeded that of the CJ velocity as shown in Figure 2c. This flow condition corresponded to a velocity ratio of 1.27, i.e. H2-Air free-stream Mach number of 6.46. By reducing the H2-Air velocity below that of CJ velocity, unsteady detonation was produced behind the bow shock as depicted in Figures 2a and 2b. These conditions corresponded to velocity ratios of 0.82 and 0.94, respectively, and associated combustion oscillations were on the order of 150 and 720 kHz. While all three test cases have been utilized by researchers for CFD model validation, the current work was focused solely on the steady shock-induced combustion condition of M=6.46.

Figure 3 provides a schematic of the general flow structure observed in the steady shock-induced combustion problem. Two strong discontinuities in density were generated by the supersonic flow of premixed, stoichiometric H2-Air. The first was a characteristic bow shock that formed ahead of the 15 mm diameter projectile. Behind the bow shock, a second stationary wave was observed in the form of a weaker discontinuity. This discontinuity was due to combustion being initiated by the increase in pressure and temperature behind the bow shock. The distance between the shock and the flame front is commonly referred to as the induction zone. In the region close to the nose of the projectile, the bow shock was strongest resulting in a closely coupled flame front that was nearly indistinguishable from that of the shock wave. Moving radially outward, the bow shock weakened as indicated by the reduction in shock angle. Since chemical time scales associated with detonation initiation are pressure and temperature

dependent, the combustion delay time and associated induction zone grew as the bow shock weakened. Eventually, the flame front completely decoupled from the bow shock, as the shock strength was insufficient to initiate a detonation. As just described, the fundamental characteristics of this test case allow for unique evaluation of the suitability of chemical mechanisms in simulating stoichiometric H2-Air detonation. Specifically, the location and shape of both the bow shock and flame front provide practical indications of whether the heat release and chemical induction-delay times are accurately reproduced by the finite-rate chemistry CFD methodology.

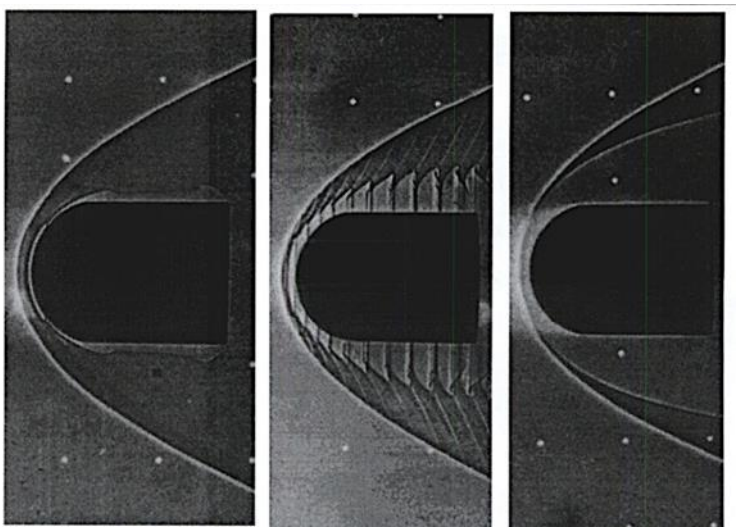

Figure 2: Lehr's Experimental Shadowgraph Visualizations of H2-Air Shock-Induced Combustion Modes (a) M=4.18, (b) M=4.79, (c) M=6.46 (steady) [Ref. 12]

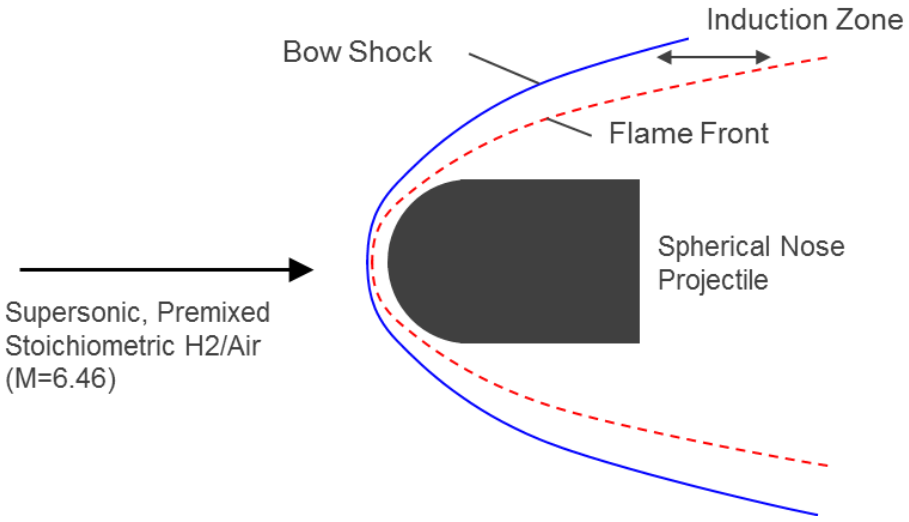

Figure 3: Steady Shock-Induced Combustion over a High Speed Projectile

B. Preselection of Chemical Mechanisms

A literature survey was conducted to preselect a series of reduced chemical mechanisms for modeling detonation of H2-O2-N2 mixtures. While numerous papers have been published over the years regarding this subject, James Clutter [13] has compiled a detailed review of computational efforts in modeling shock-induced H2-Air detonations. In his work, numerous chemical mechanisms were discussed, which ranged from two-step global mechanisms to more detailed 32-step mechanisms that included nitrogen reactions. Clutter expanded upon the reported studies by performing further numerical studies for the M=6.46 Lehr test case. Upon review of his work and others, six finite-rate chemistry mechanisms were selected for investigation in the current study. These mechanisms are summarized in Table 2. In addition to the Lehr shock-induced combustion problem, researchers have also implemented these mechanisms for the purposes of modeling other detonation problems [21, 22].

Table 2: Pre-Selected Mechanisms for H2-O2-N2 Detonation Modeling

Mechanism	# Species, # Reactions	Comments
Shang [14]	7s, 7r	Reduction of Drummond [15] by removal of HO2 and H2O2
Evans & Schexnayder [15]	7s, 8r	
Drummond [16]	9s, 18r	Some rates modified by Ahuja & Tiwari [17]
NASP [18]	9s, 19r	
Jachimowski [19]	9s, 20r	
Jachimowski + Warnatz [20]	9s, 19r	H+O2→OH+O rate modified as suggested by Warnatz

C. CFD Model

The axisymmetric solver of the Loci/CHEM code was implemented for the Lehr test case. Since shock locations were known from experimental shadowgraphs, the size and shape of the CFD domain could be optimized to minimize the number of computational cells in the model. The inflow boundary was positioned such that it was slightly larger than 2.5 times the experimental distance of the shock wave to the noise tip, which was roughly 1.35 mm. The inflow boundary also followed a basic arc profile away from the projectile permitting the bow shock to be captured with minimum excess free-stream flow. The length of the domain extended to the end of the projectile, but did not include the wake region. Truncating the domain at this location allowed for an extrapolation boundary condition to be imposed in the simulations. The mesh spacing was refined until convergence in the bow shock location was observed in the simulation results. The mesh resolution study was conducted with the NASP 9s/19r mechanism, and the final mesh spacing is shown in Figure 4 below. This final converged mesh was similar to that used by other researchers for this test case and constituted approximately 7 points per induction length (i.e. dx = 1/7 * 0.15 mm) for H2-Air at stoichiometric conditions. Inviscid walls were assumed for the projectile, as the boundary layer was not relevant to the test case. The inflow conditions imposed were those reported by Lehr, namely: M=6.46, P=0.42 atm, T=292K, and stoichiometric H2-Air mixture.

The inviscid fluxes of the Navier-Stokes equations are solved using a flux-difference-splitting-technique within the finite-volume framework of the Loci/CHEM code. Monotonic solutions around flow discontinuities such as shock waves are achieved using flux gradient limiters. Two limiter choices exist within Loci/CHEM: Barth [23] and Venkatakrishnan [24]. The Barth limiter is commonly used for unstructured meshes due to its robustness in preventing overshoots. The Venkat limiter is a thresholding limiter that is strongly enforced in areas of larger perturbations but relaxes in areas of relatively smooth flow conditions. The result of the thresholding limiter is better convergence rate and higher accuracy. Therefore, to provide the best possible shock capturing in the simulation, the Venkat limiter was imposed. However, due to carbuncle issues that Roe-based schemes have with slowly moving normal shocks, such as the bow shock, an adaptive approach was used for the approximate Riemann solver [25]. Specifically, the Roe scheme was used in most regions but the slightly more dissipative HLLE algorithm [26] was applied in locations of strong pressure jumps. Within a computational cell, the criterion for transitioning from Roe to HLLE was based on the local pressure gradient exceeding a specified value. To achieve steady-state convergence in the simulations, the implicit, second-order time-accurate method of Beam and Warming was utilized. A time-accurate integration method was selected primarily to maintain consistency with follow-on transient detonation simulations. For the Lehr test case, the time step specified was 1e-7 seconds. This corresponded to a CFL number less than 10 within the domain. Each time step consisted of nine iterations for both the Gauss-Seidel linear solver and the Newton time integration.

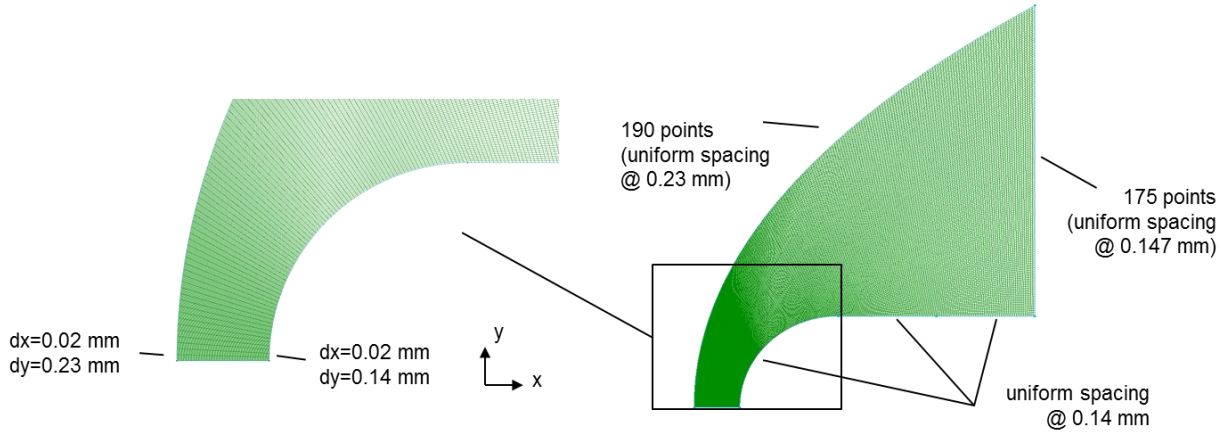

Figure 4: Structured Mesh used for Modeling Lehr Test Case

D. Results

Each of the six chemical mechanisms identified was used to model the H2-Air shock-induced combustion problem with a free-stream Mach number of 6.46. The experimental shock and flame front locations were plotted along with the predicted density contours for each mechanism in Figure 5. While all mechanisms correctly captured the standoff distance of the bow shock near the noise of the projectile, the results show that only the two seven-species mechanisms (Shang and Evans) captured the shape of the bow shock away from the projectile. The experimental data showed a “rolling” off of the bow shock due to the decoupling of the flame from the shock as the radial distance away increased. The seven-species models produced reasonable heat release and induction lengths as a function of the shock pressure rise in order to correctly reproduce the experimental shock-flame fronts. However, the nine-

species models produced shock and flame fronts that continued to remain coupled creating a constant angle “oblique” detonation wave. This sustained detonation appeared to be due to excessive heat release with little or no change in induction length even as the distance away from the projectile increased. It is important to note that these observations are consistent with previous published works using these mechanisms. Also, the seven-species Shang mechanism is a reduction of the Drummond mechanism by removal of HO2 and H2O2 species. This might explain why the Drummond mechanism appeared to be the more accurate nine-species mechanisms tested in this study so far.

Upon review of these predictions, the author proposed modifying the molecular hydrogen/hydroxyl reaction (H2+OH=H+H2O) for all nine-species mechanisms to have a consistent Arrhenius pre-exponential constant (An) of 2.16×10^6 gmol/cm^3. This is essentially a two-order reduction in magnitude (e.g. NASP = 2.16×10^8) and would put it of the same order of magnitude as the Shang mechanism (3.16×10^6). The proposed modification resulted from a series of systematic sensitivity studies to ascertain the primary reaction causing the excess heat release. It was believed that there was a common cause for the inability of the nine species mechanism to produce the correct shock induced combustion condition. The results from the sensitivity study suggested the hydroxyl reaction identified above was the critical reaction and required a reduction in its rate constant. Figure 6 shows the resulting predictions for the modified nine-species mechanisms in addition to the original 7-species mechanisms. The results indicate that by reducing this reaction rate, consistent agreement between the predictions and experimental shock-flame fronts were obtained for all mechanisms. The only mechanism that exhibited significant issues was the modified Jachimowski mechanism. This mechanism developed numerical instabilities in the form of oscillations in the flame front near the nose of the projectile. Eventually, the instability grew until the solution diverged. However, the other modified mechanisms were numerically stable but with very small “waviness” being exhibited well behind the shock front. This could have been a result of insufficient mesh/time-stepping to maintain control of the solution with the nine-species models. Further study into the ramifications of the proposed modification was therefore necessary.

Figure 7 provides a more quantitative comparison between the original seven-species mechanisms and the modified nine-species mechanisms by presenting axial plots of density and temperature at two radial locations. Essentially the same peak and post combustion densities were produced by all mechanisms. The Mach number distributions, not shown, produced similar results as well. In general, the Drummond 9s/19r mechanism was consistently the “average” of all the other mechanisms. Near the nose of the projectile, the Shang 7s/7r and the Drummond 9s/18r mechanisms produced practically the same results. At the radial offset distance of 15 mm, differences between the seven and nine-species mechanisms became more evident. The two seven-species mechanisms were quite similar in density and temperature profiles, while the modified nine-species mechanisms produced slightly larger induction zones. The modified NASP mechanism produced the largest induction zone with an elevated temperature in the oblique detonation region. No experimental data was available for validating the temperature/density fields, so no judgment can be made regarding the quantitative accuracy of each mechanism. Overall, the seven-species and the stable modified nine-species mechanisms performed well in capturing the flow structure of the shock-induced combustion test case. Therefore, the mechanisms were down-selected to one seven-species and one nine-species mechanism for further study, namely the Shang 7s/7r and the modified Drummond 9s/18r mechanisms.

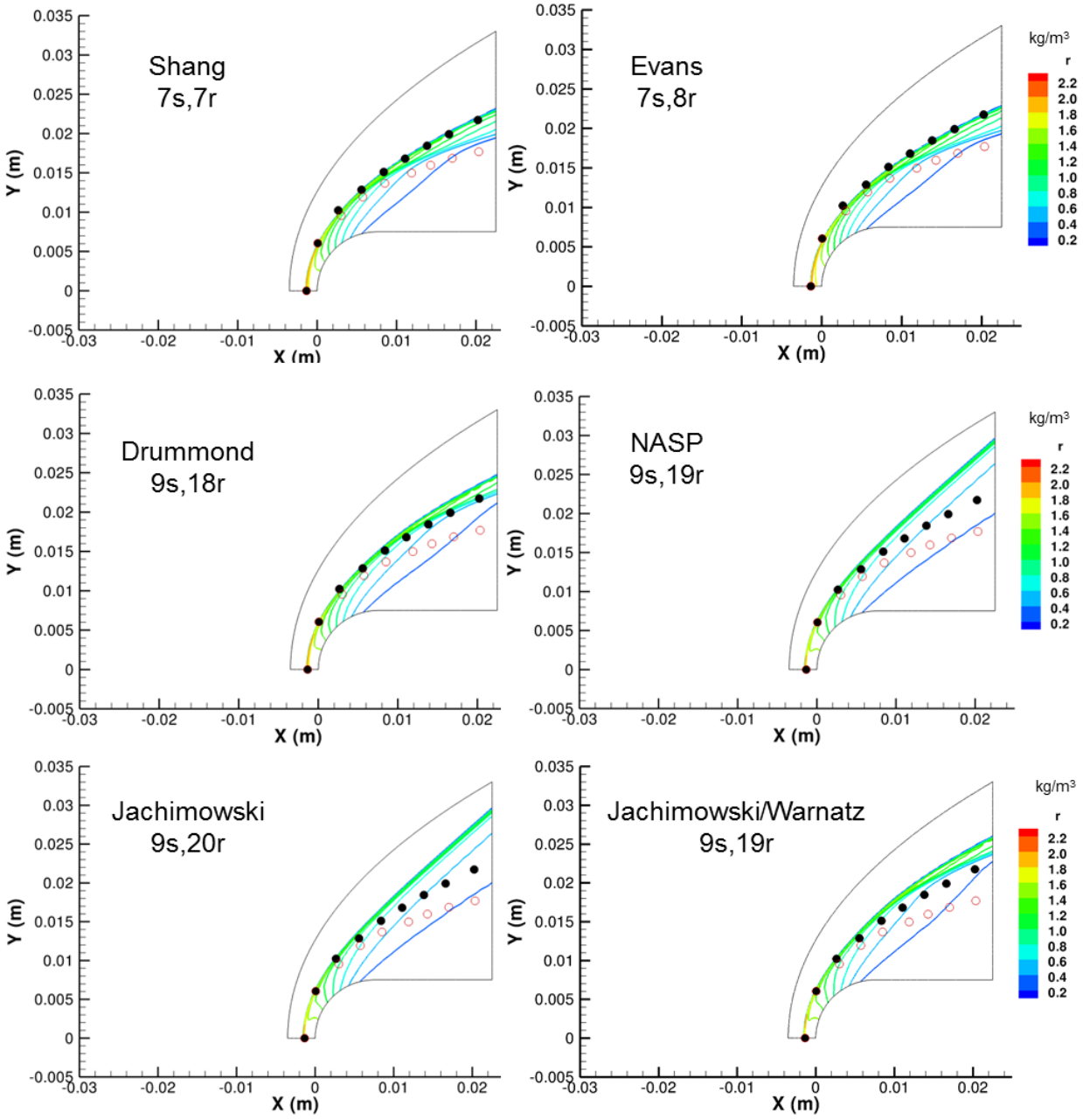

Figure 5: Density Contours Using Pre-Selected Chemical Mechanisms

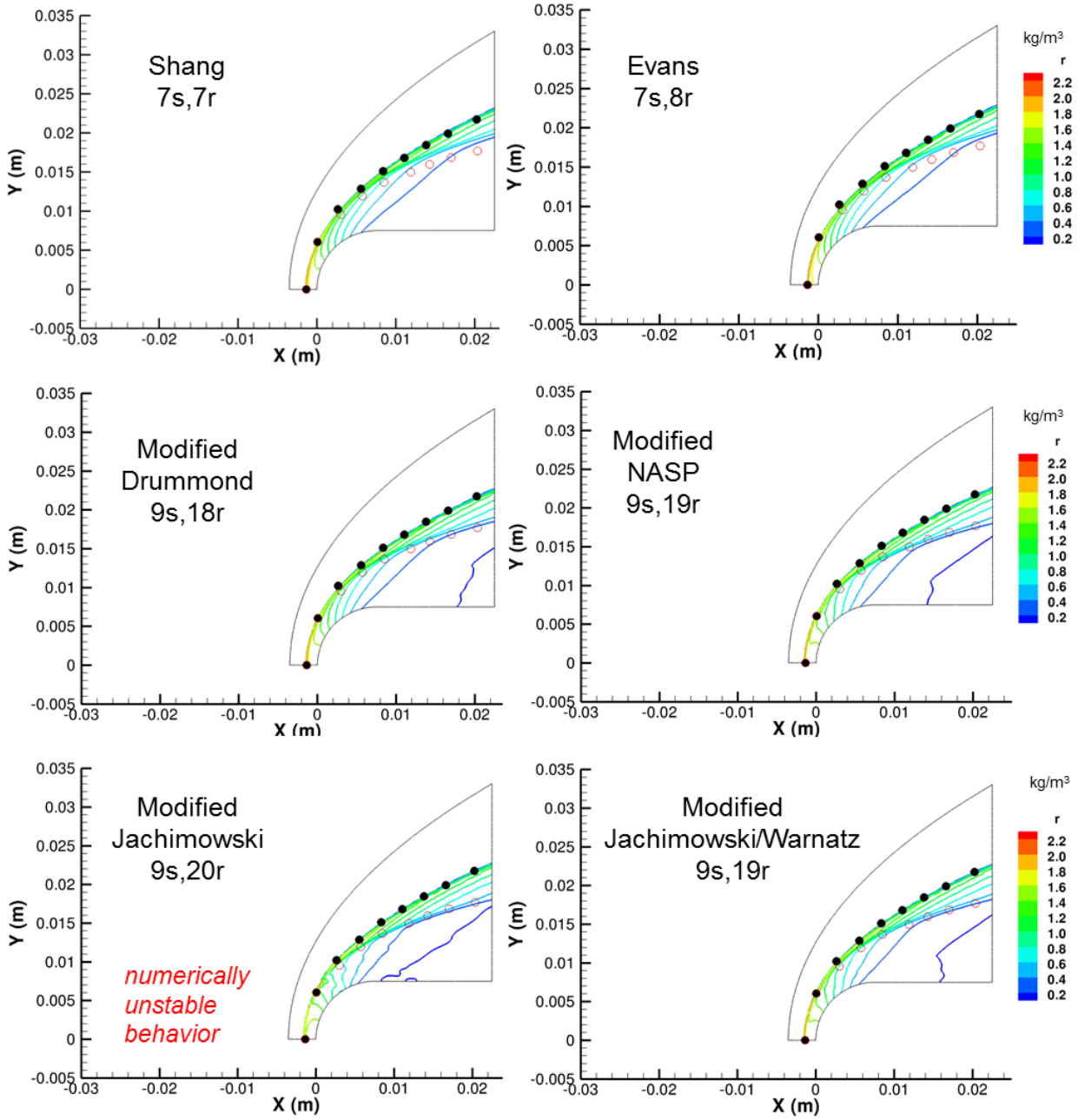

Figure 6: Density Contours Using Proposed Modifications to the 9-Species Mechanisms

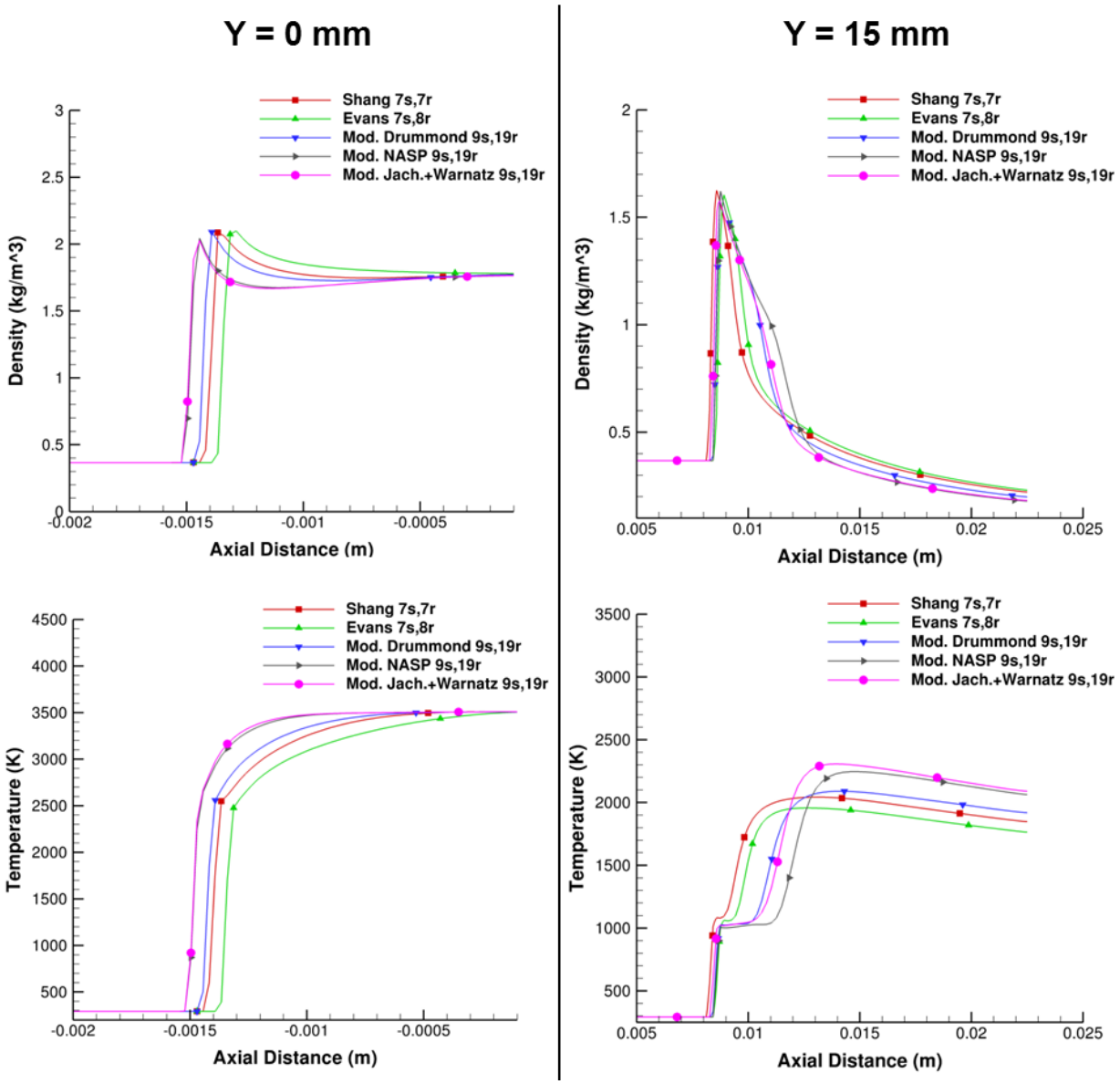

Figure 7: Axial Profiles of Density and Temperature for Two Radial Locations (a) y=0 and (b) y=15mm

V. Planar H2-Air Detonation Wave Verification

A. Background

A common test case for detonation model verification is the planar detonation wave propagating in a shock tube. This quasi-1D problem provides a means to verify that the theoretical Chapman-Jouguet (CJ) conditions are being predicted by the CFD tool with the selected chemical mechanism. The transient simulation also allows for characterizing spatial and temporal modeling requirements for numerical methods being implemented and ascertaining the extent of dissipation/dispersion errors.

H2-Air at stoichiometric conditions was selected as the detonable mixture, and the CJ conditions are given in Table 3 below. These values were generated using the NASA Chemical Equilibrium Analysis (CEA) program [27]. For the purposes of this report, standard temperature and pressure for the initial conditions of the detonable mixture were taken to be the conventional thermodynamic reference state of 298 K and 1 atm. Using the CJ detonation Mach number and standard normal shock relations, the Von-Neumann peak pressure of the detonation blast wave was computed to be approximately 27.3 bar for both true and theoretical air. Theoretical air is the theoretical mixture of 23% O2 and 77% N2 by mass, while "true" air is assumed to be composed of approximately 75.52% N2, 23.14% O2, 1.29% Ar and 0.05% CO2 by mass.

Table 3: Theoretical CJ Conditions for Stoichiometric H2-Air at 298 K, 1 atm

	H2 + Air	**H2 + Theoretical Air** *(By Mass: 23% O_2, 77% N_2)*
Pressure (bar)	15.71	15.68
Temperature (K)	2947.1	2942.7
Density (kg/m^3)	1.536	1.532
Specific Heat Ratio (-)	1.163	1.163
Sound Speed (m/s)	1090.7	1091.2
Mach Number *Lab Frame of Reference	4.819	4.816
Wave Speed (m/s)	1967.7	1968.6
Mass Fractions		
H_2O	0.22100	0.22188
N_2	0.72932	0.74058
OH	0.01350	0.01360
H_2	0.00274	0.00265
O_2	0.00963	0.01015
Ar	0.01255	-
Von-Neumann Pressure (bar)	*27.29*	*27.25*

B. CFD Model

Figure 8 provides general schematic of the CFD domain for the planar detonation model. It consists of a 1D shock tube filled with perfectly mixed stoichiometric hydrogen and air at standard atmospheric temperature and pressure. A relatively small zone of high pressure and temperature was used to directly initiate the detonation without the need of shock-focusing or turbulence generating devices. The shock tube was of sufficient length for the detonation to initiate and stabilize to a steady propagation speed, i.e. transient "self-similar" conditions whereby the CJ conditions could be ascertained. An appropriate initiation zone was determined to be approximately 10 induction lengths in size, or 1.5 mm. Within this initiation zone, temperature and mass fractions were set equivalent to the CJ state, while pressure was elevated to be twice that of the CJ state, i.e. $2*P_{CJ}$=30atm. These conditions helped ensure prompt detonation without generating excessive overdriven shock waves.

The Loci/CHEM solver settings used for the planar verification problem were the same as those described in the Lehr shock-induced combustion problem. All the chemical mechanisms studies in the Lehr case were implemented for this test case as well. However, due to the similarity in the results, only the Shang 7s/7r and Modified Drummond 9s/19r mechanism results were presented. The effect of the mesh resolution in capturing the CJ conditions for the planar detonation problem was demonstrated by simulating on both a coarse and highly refined

structured 2D mesh. The coarse mesh consisted of a uniform spacing of 0.5 points per chemical induction length, i.e. 0.3 mm spacing. This coarse mesh, with insufficient resolution for capturing the induction zone, was selected for the purposes of evaluating its capability in capturing a self-sustaining planar detonation wave with the proper CJ state conditions. The refined mesh had a uniform spacing of 30 points per chemical induction length, i.e. 0.005 mm spacing. The refined mesh provided a representative mesh-independent solution for comparison. With the use of reduced chemical mechanisms, a minimum of 10 to 20 points per induction length should be required to accurately capture the induction zone. As a point of reference, the Lehr validation study presented earlier in the report demonstrated that a mesh resolution of 7 points per induction length provided sufficient resolution to obtain mesh-independent results.

A time step of 1e-7 seconds was used in the simulations. This time step was deemed the maximum acceptable value for the current test case based on resolving combustion time scales of interest. A critical combustion time scale for the planar detonation wave can be estimated by considering the smallest associated combustion length-scale (e.g. induction zone) and the speed at which it propagates through the mixture (i.e. burned gas acoustic speed). Therefore, the planar detonation wave has a critical combustion time scale of approximately 1.37e-7 sec (0.15 mm/1091.2 m/sec). In regards to gas dynamics, or shock propagation, time scales are governed by the detonation wave speed and selected mesh resolution. In the next section, the sensitivity of mesh spacing in resolving the shock propagation will be discussed for a fixed time step of 1e-7 seconds.

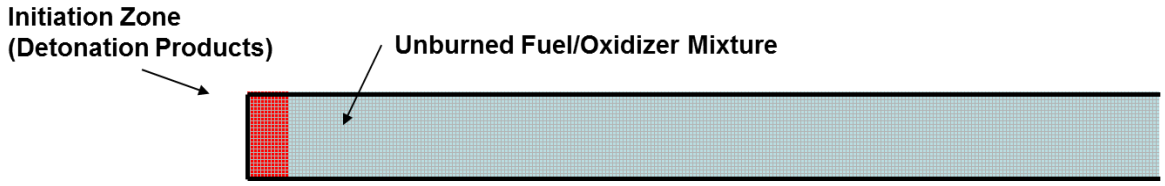

Figure 8: Schematic of the Initiation of a Planar Detonation Wave

C. Results

During the current work, it was determined that a self-similar detonation wave was established within 0.3 m downstream from the closed-end of the shock tube using the coarse mesh. This behavior was consistent for all chemical mechanisms studied. Therefore, to ensure consistent detonation wave profiles were being obtained for comparison, each simulation ran for 3000 iterations at a time step of 1e-7sec, i.e. 0.3 msec. This translated into the detonation wave being located approximately 0.6 m downstream due to the wave speed being on the order of 2 km/sec. Figure 9 provides the profiles of pressure, temperature, density and H2O mass fraction with respect to axial location for the coarse mesh, where the values have been normalized using the NASA CEA computed CJ state conditions. The results for both the Shang and the Modified Drummond mechanisms are given in Figures 9a and 9b, respectively. By normalizing the CFD computed values with their corresponding CJ conditions, the existence of a CJ state could be ascertained, as there should be a common point at which they all equal one. Figure 9 depicts that this occurred for both mechanisms using the coarse mesh. All flow properties converged to a value of one indicating the coarse mesh resolution was sufficient for the mechanisms to capture the coupled flame-shock combustion process. In these figures, the pressure profiles have also been plotted by normalizing the computed values with the theoretical von-Neumann spike pressure (P_{vn}). This normalized pressure peaked at a value close to unity depicting the

leading shock strength is consistent with that of a theoretical planar detonation wave for both mechanisms. No significant differences were observed between the Shang and Modified Drummond mechanism that would indicate the need to use the large mechanism set of 9-species and 18-reactions.

Despite the fact that the very coarse mesh was able to predict some of the basic thermodynamic properties of a coupled shock-flame front, a refined mesh simulation showed there are errors in such a simulation. Figure 10 provides similar profiles as that of Figure 9 except for the refined mesh of 30 points per induction length. A few observations can be made regarding the solution of the refined mesh in comparison to the coarse mesh. First, the profiles are much smoother with the refined mesh indicating some increased amounts of dispersion errors were present with the coarse mesh. Second, higher peak values occurred with the refined mesh due to improved shock capturing, and these values were consistent in magnitude for both mechanisms. However, one major difference between the coarse and refined mesh simulations was that the expansion process behind the detonation wave was fundamentally different. The decay in density/pressure was much more rapid in the refined mesh. Also, the profiles indicate the refined mesh predicted a slightly over-driven detonation wave at this location. Specifically, both the VN pressure and temperature spike were elevated upstream of the CJ location as indicated in Figure 10. This is also confirmed by plotting the computed detonation wave speeds as a function of axial distance as shown in Figure 11. Both mechanisms with the refined meshes of 30 points per induction length predicted wave speeds approximately 9% above the theoretical CJ wave speed of 1968 m/sec. Note, the wave speed reached a steady value and was not a result of an overdriven detonation. The coarse mesh wave speeds reproduced nearly exactly the theoretical wave speed. It is believed by the author that the slightly-elevated wave speeds with the refined mesh are result of insufficient solution convergence for each time step by the solver. In these simulations, a constant physical time step of 1e-7 sec was used. Therefore, considering the wave speed of the detonation as the critical velocity in the flow to resolve, the coarse mesh constituted a CFL number of 0.656, while for the refined mesh the CFL number was 39.36. This demonstrates the robustness of the Loci/CHEM code in utilizing large time steps to capture detonation events without exhibiting numerical instability issues. While future work will involve revisiting this test case and confirming the time step requirements to capture the planar detonation wave speeds to a higher-level of accuracy, these analysis results were deemed satisfactory to proceed with the verification and validation efforts.

As a final verification test for the planar detonation problem, simulations were conducted of non-stoichiometric H2-Air detonations using the Shang 7s/7r mechanism with the refined mesh. It should be noted that the induction length grows non-linearly away from the stoichiometric point. Therefore, the resolution of the induction zone varied with equivalence ratio and no attempt was made at optimizing the mesh for each non-stoichiometric condition. Figure 12 shows a plot of the variation in density, temperature and wave speed as a function of equivalence ratio. The NASA CEA predictions were provided as curves for comparative purposes. All values in the figure have been normalized by the CEA stoichiometric state condition. The results show that density and temperature were predicted well by the Loci/CHEM code for both fuel-lean and fuel-rich mixture conditions. The wave speeds were elevated for the near-stoichiometric and fuel-rich conditions. The agreement between Loci/CHEM and NASA CEA wave speed predictions improved with fuel lean conditions as the detonation wave speed decreased. Since this translates directly to a reduction in the solver CFL number, this is consistent with the previous assertion that the errors in the wave speed predictions were attributed to errors in temporal convergence. It is important to note that from this point on, all modeling efforts presented in this report utilized the Shang 7s/7r mechanism. No further examination or comparison of other chemical mechanisms will be presented.

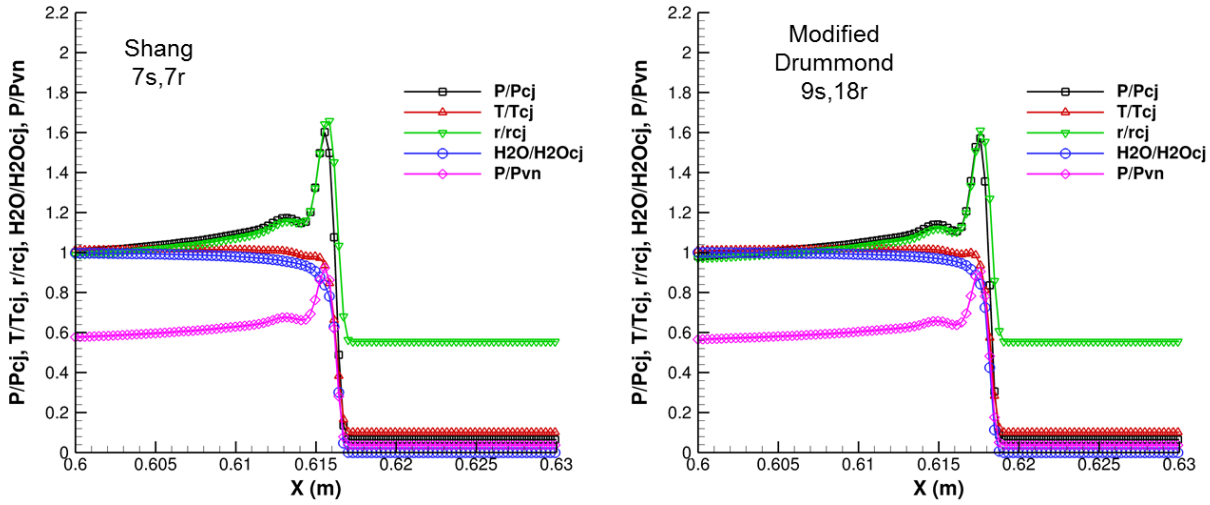

Figure 9: Stoichiometric H2-Air Detonation Wave Profiles at a Mesh Resolution of ½ Point per Induction Length (Values Normalized by Stoichiometric CJ Properties)

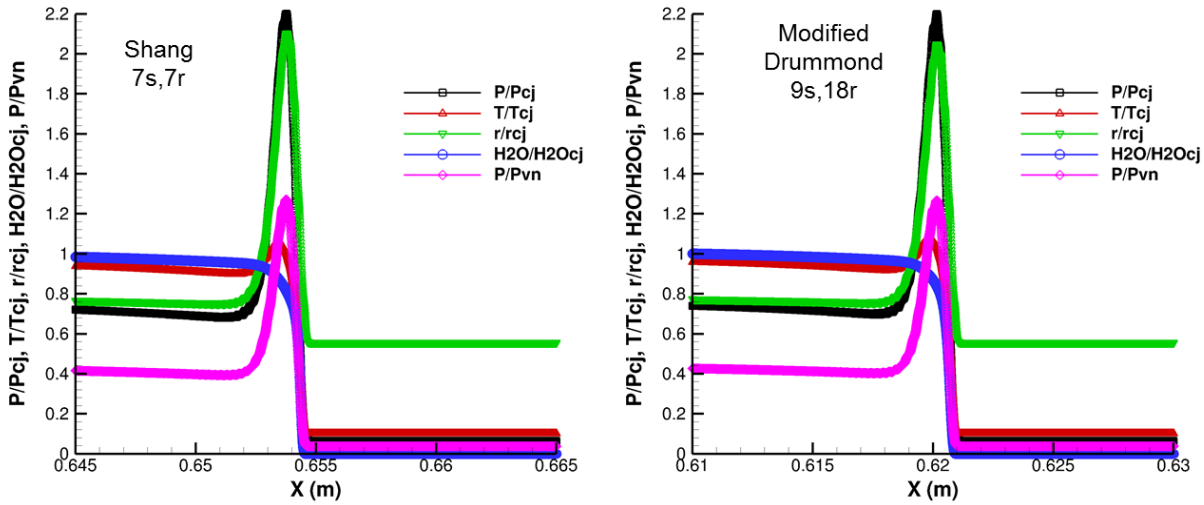

Figure 10: Stoichiometric H2-Air Detonation Wave Profiles at a Mesh Resolution of 30 Points per Induction Length (Values Normalized by Stoichiometric CJ Properties)

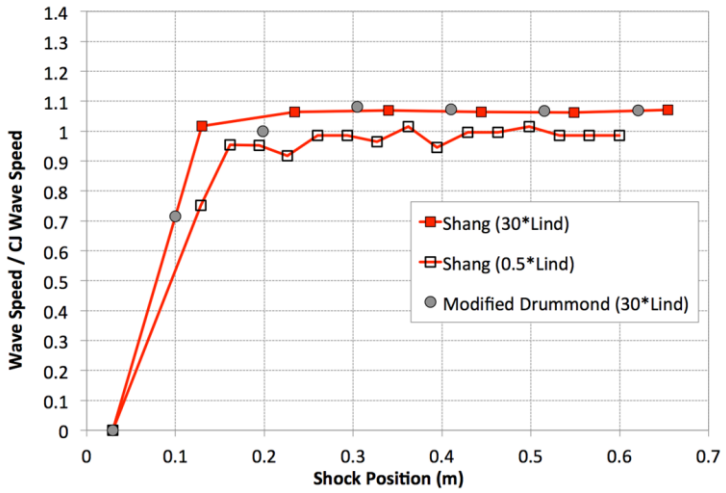

Figure 11: Comparison of Stoichiometric H2-Air Detonation Wave Speeds

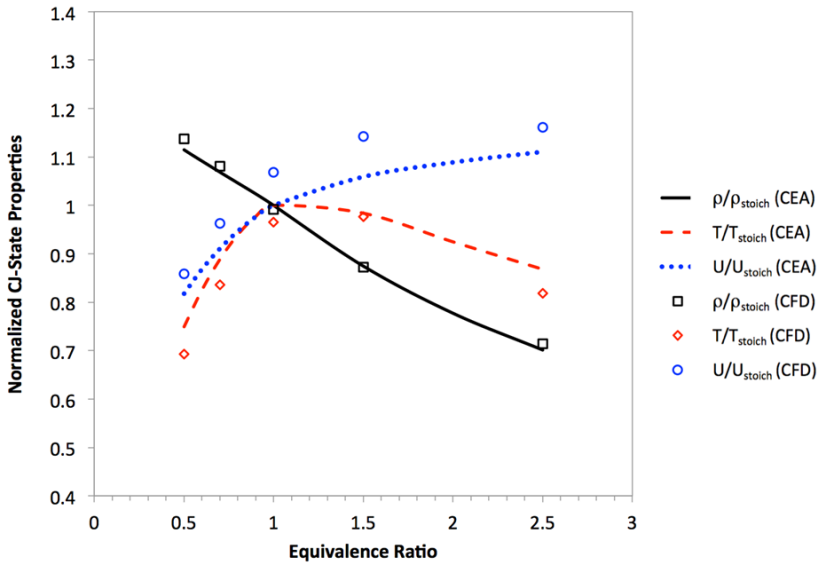

Figure 12: Prediction of Non-Stoichiometric Detonation Wave Conditions of Original 30*L_{ind} Mesh (Values Normalized by Stoichiometric CJ Properties)

VI. Spherical Vapor Cloud Explosion (VCE) Verification

A. Background

Previous verification and validation tasks in this report were focused on predicting detonation events that occurred with some interaction with solid walls. For rocket propulsion testing, some portion of the detonation event might occur in open-air environments without any structures interacting or confining the blast event. Thus, verification of the current modeling approach was needed to show that it was capable of predicting both the source and blast-propagation of an open-air detonation event.

The current NASA engineering-safety methodology for assessing open-air propellant detonations is generally to equate vapor cloud explosions to "equivalent" high-density explosives such as TNT. By properly equating the gaseous detonation to TNT, empirical blast curves can then be used to determine peak pressures and impulses as a function of distance from the center of the vapor cloud [40]. This methodology is referred to as the TNT equivalency approach and is typically used for determining quantity distance for personnel and facility safety. One of the challenging aspects of this approach is determining the appropriate "equivalent" yield of TNT. In the case of a liquid-hydrogen/liquid-oxygen mixture for example, the NASA Standard 8719.12 [41] recommends that the explosive equivalent weight be the larger of the following two values: $8*W^{2/3}$ or 14%*W, where W is the LO2-LH2 weight. The two-thirds power relation has been reported to be a result of the competition between the surface area and volume of a propellant tank rupturing [42]. The proportionality factor of eight was selected to ensure conservative estimates for human safety. Historically, the method prior to this standard was to assume the equivalent TNT mass to be a fixed percentage of the propellant mass detonating [43]. In the case of static test stands with LO2-LH2 propellants, the yield was assumed to be 60%. According to the report, this corresponded to roughly within five percent of equating the energy released by the chemical explosion to the higher heating value of the propellant. As will be shown later, this particular approach appears to correlate with assuming CJ pressure at the edge of the vapor cloud that then decays radially at the equivalent TNT far-field rate. An alternate approach to equating the chemical detonation to an equivalent TNT source is to derive the energy released based on converting the pressure energy of the original state of the propellant gas to the potential energy required to bring it to the detonation state. This method has been outlined by Strehlow and Baker [45] as well as others. The proposed equation for the energy released based on the volume of propellant is shown in equation 1 below. The benefit of this approach is that neither an assumption of percent yield nor an ad-hoc equating of mass is needed. It simply uses an energy balance to derive an "equivalent" mass of TNT combined with standard TNT curves to estimate the radial decay in overpressure and impulse.

$$E_o = \frac{(P_{CJ} - P_o) * V_o}{\gamma - 1} \qquad \text{Eq. 1}$$

A fundamentally alternative approach recently implemented at NASA Stennis is a semi-empirical method of modeling the source using appropriate conservation equations to determine the detonation CJ properties, and then propagating the air-blast through the near, mid and far-field regimes using specific semi-empirical relations. This methodology was successfully applied by Allgood [44] in the prediction of blast environments produced by ethylene-oxygen, pulse detonation engine experiments. While it is consistent with the commonly used methodology outlined by Strehlow and Baker [45] of honoring the total energy released from the detonation and not requiring an ad-hoc equivalency factor, it differs in that it does not use the TNT empirically derived propagation curves. Rather, the blast-propagation is performed by segmenting the spherical blast into either a strong-shock or weak-shock regime as described by

Sedov [46] and Raspet [47]. Thereby, this modeling approach completely removes the assumption of equating the vapor cloud explosion to a high-density “point-source” explosion.

B. CFD Model

In order to simulate a spherical open-air detonation event with a minimum CFD domain size, symmetry in the problem was utilized by considering a 30-degree spherical segment. The volume mesh was achieved through the following extrusion process. First, a grid line was rotationally extruded in 1-degree increments about a centroid axis. This created a 30-degree surface mesh in one plane. The surface mesh was then rotationally extruded about a second centroid axis in 1-degree increments to create the final volume mesh.

To further reduce the CFD domain size, the modeling was conducted using a set of two meshes. The first mesh, or source model, was used to simulate the source of the detonation event. The philosophy was to limit the source model in its radial size to include the mixture of H2-Air as well as some portion of surrounding air outside the vapor cloud. This would allow for maximizing the grid resolution during the detonation process while minimizing the number of grid cells in the CFD model. After the detonation was allowed to consume the entire propellants and the remaining air-blast had propagated sufficiently far away from its source, the solution could be interpolated onto a second mesh where the mesh spacing had been relaxed for more efficient computation of the air-blast propagation. Typically, allowing the blast wave to consume on the order of 10 times its original volume enabled a sufficiently decoupled shock wave, where the mesh resolution requirements became independent of the detonation event.

In the current task, the source model consisted of a 1 m radius of air. Inside this domain, a 0.5 m radius of stoichiometric H2-Air mixture was imposed at STP. The detonation was initiated directly at the center by a 10 mm radius of H2O at 47.25 atm, or three times the CJ pressure, and a temperature of 3000K. The initiation pressure was increased above the $2xP_{CJ}$ conditions used in the planar detonation problem to ensure direct initiation in the three-dimensionally expanding gases. The source model consisted of a 0.3 mm uniform radial spacing of grid points resulting in an approximate total cell count of 3 million for the structured mesh. The propagation model consisted of a 10 m radius domain of air at a 2 mm radial mesh resolution. This resulted in a cell count of 4.5 million. Full chemistry was maintained in the propagation model, although an equivalent perfect gas approximation could probably have been utilized with minimum loss in accuracy. The current work did not investigate the implications of making such an assumption or ascertaining when such assumptions could be made. However, this is a topic which should be addressed in future work to further optimize the modeling approach as the number of equations would be greatly reduced and the assumption of frozen species would eliminate the computational overhead of modeling reactions.

The spherical vapor cloud explosion model utilized the 7s/7r Shang mechanism and similar solver settings as those used in the planar detonation case. Only two modifications to the solver settings were specified to help improve stability in the simulations. Namely, the Barth limiter with pure HLLE inviscid flux terms was used instead of the Venkat limiter with localized HLLE fixes. This made the simulation more numerically stable in modeling the higher-pressure initialization of the detonation and the three-dimensional expansion processes. Use of the Barth limiter is recommended in the BLAST module of the Loci CFD tool suite in order to capture the coupled shock-flame fronts of high-density explosives. This modification was kept for all future analysis tasks as well. As in the previous analysis tasks, the gases were assumed to be calorically imperfect with species-dependent variable specific heats and viscosities. Although not critical to this analysis, turbulence was also simulated in the model using the BSL model.

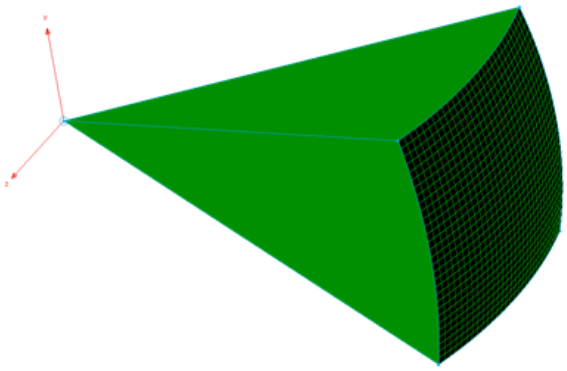

Figure 13: 30-degree Segment Mesh Topology for Spherical VCE Model

C. Results

For the source model, a series of temperature and pressure contours of the VCE have been plotted in Figures 14 and 15. The first set shows the detonation wave inside the vapor cloud at 0.1 msec after ignition. It is evident that in the temperature and pressure contours that a fully coupled shock and flame front had been established. Moreover, the flow properties indicated that the detonation wave had fully developed at this point with the wave speeds exhibiting a self-sustained behavior. At 0.3 msec after initiation, the detonation wave had reached the outer edge of the vapor cloud and a decoupling of the flame front from the leading shock had begun. Figure 15 continues the time series, depicting the cooling of the combustion gases by an expansion wave generated in the wake of the spherical air-blast. By 0.8 msec, the air-blast reached near the end of the source domain and the expansion wave had completely propagated through the combustion gases. It was at this point that the solution was transferred to the propagation mesh to continue the simulation at larger radial distances.

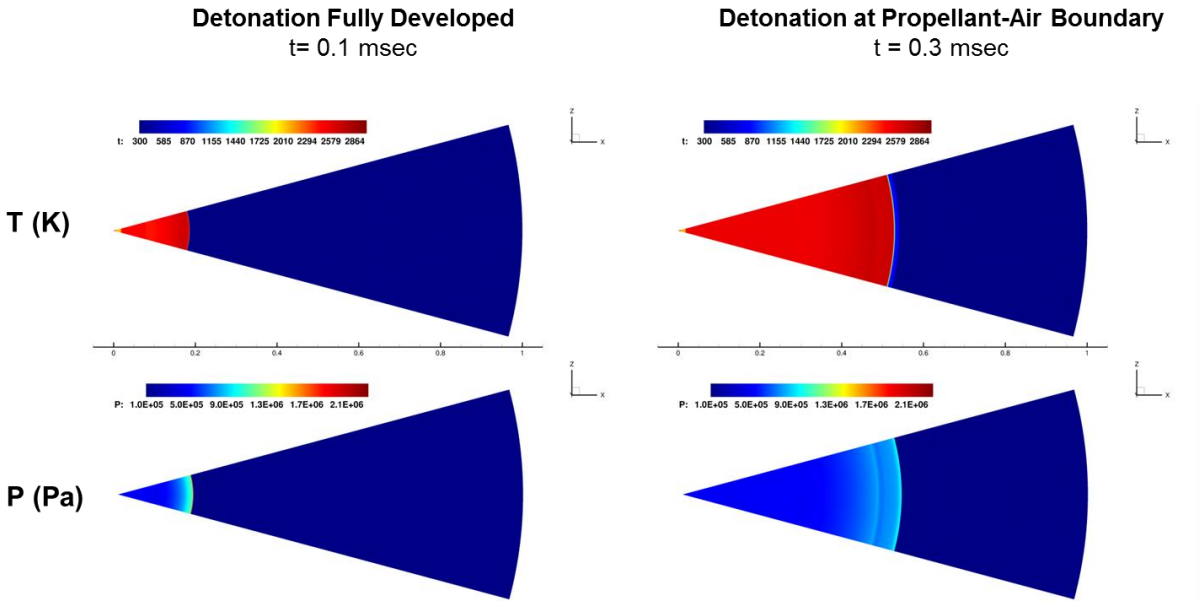

Figure 14: Temperature and Pressure Contours for Source Model during Detonation Initiation and Propellant Consumption Phases

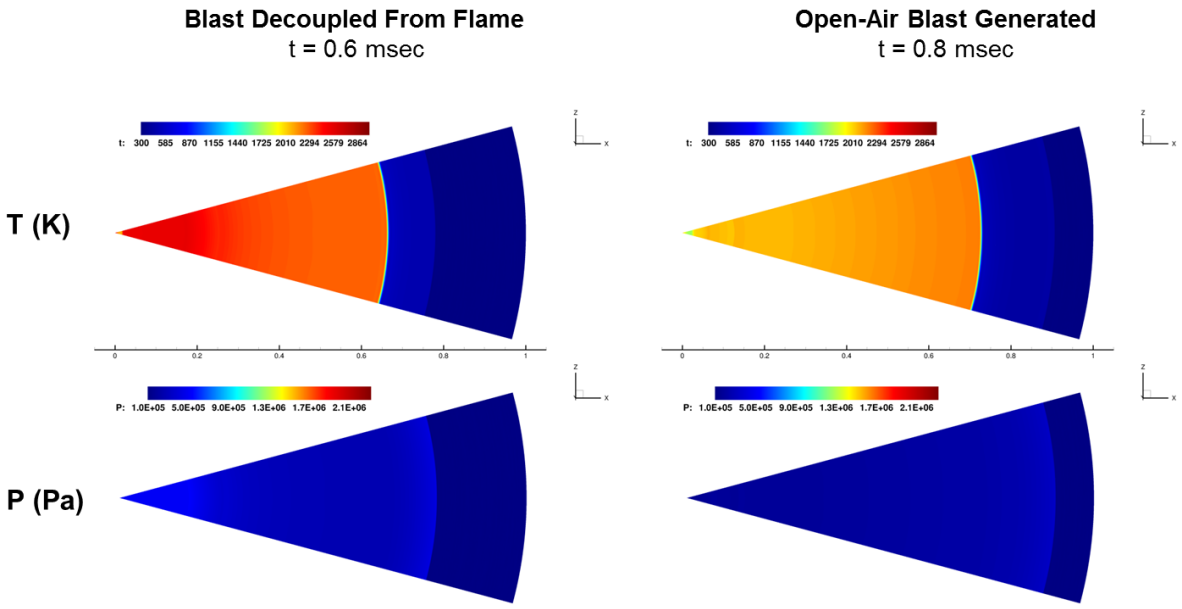

Figure 15: Temperature and Pressure Contours for Source Model during Detonation Wave Decoupling and Air-Blast Generation Phases

Verification of the VCE CFD model is best ascertained by comparing the results for the radial decay in peak pressure to those provided using TNT equivalency curves. Figure 16 is a plot of the open-air peak pressures as a function of radial distance. The NASA Standard 8719.2 recommended yields of $8*W^{2/3}$ and 14% have been included in Figure 16 along with the historical 60% weight assumption. The $8*W^{2/3}$ equivalency is obviously quite conservative as it does not properly represent the VCE as mentioned earlier. The older historical 60%*W equivalency appeared to capture the peak pressure at the edge of the VCE and is slightly conservative in the far-field. The 60%*W also was nearly identical to the potential energy based approach, which required no assumption regarding a percent yield to derive the equivalent TNT mass. The 14%*W assumption agreed very well in the mid and far-field regimes to the CFD predictions, but under predicted the peak pressures near the edge of the VCE. The SSC analytical model results are also plotted in Figure 16 for comparative purposes. This model provided the best overall agreement with the CFD and furthermore required no assumption on percent-yield or correlation in any way to a TNT explosion. The radial location, at which the transition from the 0.3 mm resolution source model to the coarser 2.0 mm resolution propagation model was made, has been indicated in Figure 16. This transition occurred in a region sufficiently far away from the edge of the VCE but prior to reaching the self-similar linear region of the far-field. The choice of where to make the transition and the selected resolution in the propagation model appeared to be appropriate as the solution maintained itself along the 14% yield TNT curve.

Further study in this area is needed to truly ascertain the Loci/CHEM CFD model's ability to capture VCEs. For example, sensitivities to the following parameters are of interest: (1) mesh resolution, (2) location of transition from the source to the propagation model, and (3) simplification to an equivalent perfect gas or gases during the propagation phase. For all these cases, the ability to predict the impulse or positive phase duration also needs to be quantified. Lastly, validation of the CFD tool with appropriate empirical VCE data is needed.

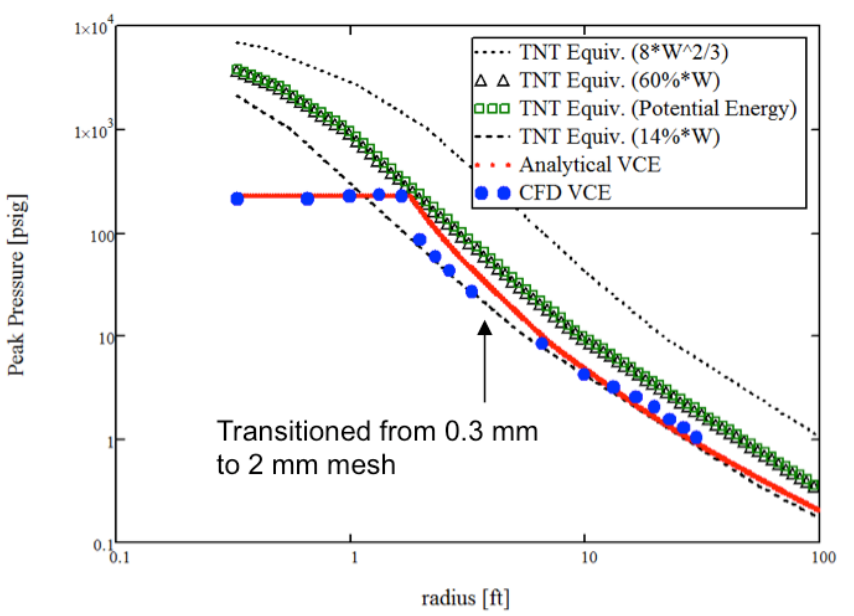

Figure 16: Comparison of CFD, Analytical and TNT Equivalency Curves for VCE of H2-Air in Open Air Conditions - Peak Overpressure vs. Radial Distance

However, prior to continuing further with these investigations, the author felt there was a need to address the following fundamental question: “How do the current modeling results of a H2-Air VCE compare to known overpressure events at rocket propulsion test facilities?” As such, three data sets were used in which high-speed deflagrations occurred in open-air. Figure 17 shows representative peak pressures from these events along with the current VCE model results. The data have been plotted in a consistent fashion by normalizing the radial distance with the cube root of the propellant weight. This is known as “scaled distance” in explosion analyses, and is the proper way to compare over-pressure events from different sized charges. All three data sets (Shuttle MPTA [48], SSC E-1 and HUCTA [49]) were known high-speed deflagration events where the flame did not transition into a detonation. Despite the fact that they were high-speed deflagrations, these events generated significant overpressure waves of the N-wave type as depicted in Figure 18 for the SSC E-1 example. Since the rocket test data correspond to deflagrations, the overpressure vs. scaled distance for these events should be much lower than that of the detonation. Figure 17 clearly shows that the current CFD model was capturing the blast wave from a detonation event, as they are substantially larger in magnitude than the deflagration data. Future work will examine the Loci/CHEM capability in predicting these high-speed deflagration events as the associated overpressures can cause catastrophic loads on facility components and launch vehicles.

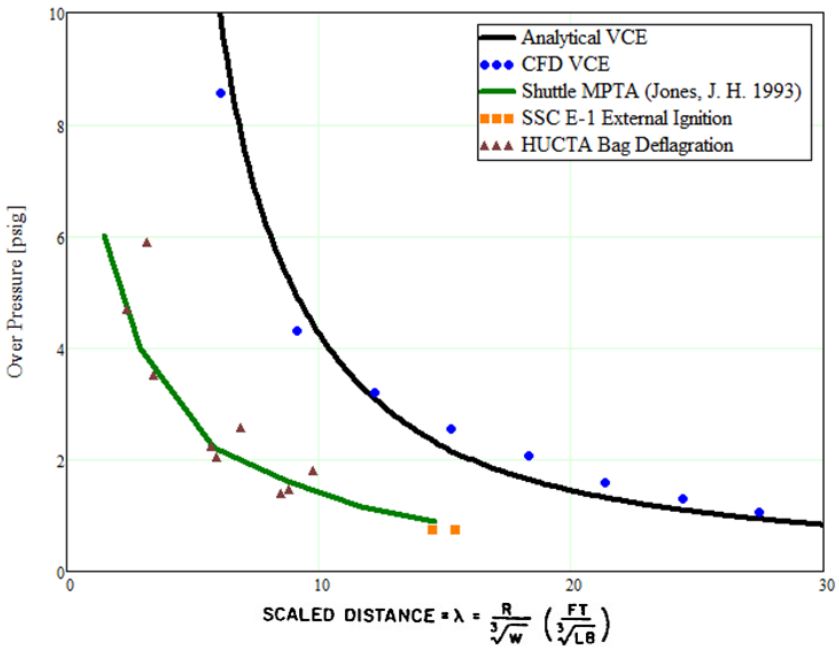

Figure 17: Comparison of CFD/Analytical VCE Predictions to High-Speed Deflagration Events at Rocket Test Facilities

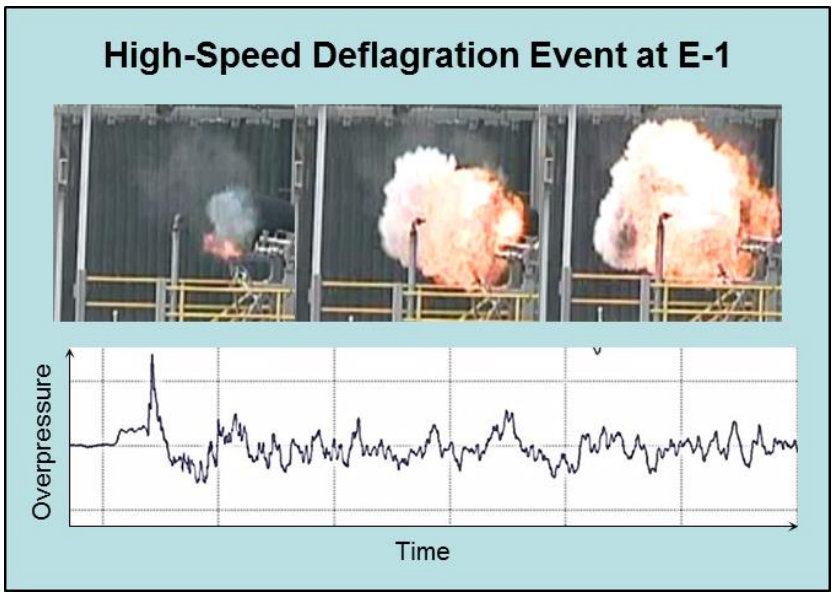

Figure 18: High-Speed Deflagration Event at NASA E-1 Test Facility

VII. Axisymmetric DDT using Orifice Plates

A. Background

All previous CFD analyses were for cases with sufficient energy to directly initiate a detonation, either from impingement of a supersonic flow on a blunt object or by expansion of high-pressure combustion gases. However, in order to confidently apply the current modeling approach to the simulation of rocket testing scenarios, the ability to reliably predict deflagration-to-detonation transition was needed. The transition from a slow-speed deflagration initiated by a low-energy spark, into a high-speed detonation is a complex process involving multiple factors. Several critical processes can control the rate of flame acceleration during the DDT process. Examples might include turbulence generated by mixing enhancement devices, pressure wave dynamics generated by reflections from solid bodies, or fluid instabilities coupled with combustion dynamics. Thus, a set of geometrically simple but relevant configurations was needed for validating the Loci/CHEM code and its ability to predict DDT.

Initially, it was desirable to select a validation case that did not involve complex three-dimensional processes but rather one in which the DDT behaved in a nearly axi-symmetrical fashion. In addition, one of the primary objectives of such a test case was to examine the accuracy of Loci/CHEM in predicting turbulent flame acceleration by coupling the BSL turbulence model and the 7s/7r Shang mechanism. Previous test cases did not address this as they were not driven by turbulent mixing but rather dominated by quasi-1D thermo-compressible flow coupling.

After examining the available literature on DDT devices, the most geometrically simplistic configuration found involved an array of circular orifice plates inside a tube. Lee et al [28] had used the test configuration shown in Figure 19 for studying DDT of various fuel/oxidizer mixtures. In the experiments by Lee, an array of orifice plates were welded at equal spacing and inserted into a detonation tube of various diameters ranging from 5 cm to 30 cm. For most configurations, the orifice plate diameter was selected to provide an area flow blockage of 43% at a pitch or spacing of 1 tube diameter. One end of the detonation tube was closed and contained a 150 mJ glow plug igniter. An inlet valve near the head end of the tube combined with an outlet at the tail end of the tube allowed for uniform filling of the tube with propellants prior to ignition. The combustion gases were allowed to escape through the outlet valve.

Depending on the test conditions, the combustion flame within the orifice or obstacle region of the tube either extinguished or reached a “steady-state” velocity. The flame extinguished when the mixture ratios were either near the fuel-lean or fuel-rich limits. In the cases where the flame did not extinguish, two regimes or combustion modes were observed. These modes were dependent upon varying tube size, blockage ratio, mixture ratio and/or propellants. The first mode was the case where the flame in the obstacle region accelerated to the isobaric sound speed of the mixture. This was characterized as the “choking” regime and occurred away from the stoichiometric point. At large tube sizes and stoichiometric mixtures, near CJ detonation waves were established inside the obstacle field. However, with smaller tube sizes, such as the 5 cm tube, supersonic combustion occurred but at a speed well below that of the CJ detonation wave speed. For example, stoichiometric H2-Air with a 5 cm tube and 43% blockage generated flame speeds on the order of 1500 m/sec inside the obstacle region. This was termed a “quasi-detonation”. The sub-CJ wave speeds were attributed to the severe momentum and heat losses caused by the orifice plates. Complete acceleration to the CJ velocity was observed to occur promptly at the end of the orifice plate region.

A similar study was also conducted by Chapin [29] who examined the use of orifice plates as DDT enhancement devices for pulse detonation engines. Chapin also investigated the same 5 cm tube diameter configuration but with a shorter row of orifice plates in order to minimize drag losses and thereby make the device more practical for propulsion applications. The primary difference between the configuration used by Lee and that used by Chapin was that the overall length of the obstacles reduced from 6 m to 0.45 m (18 inches). The configuration tested by Chapin was selected as the validation test case, as visualization of the DDT event was available through the use of a polycarbonate detonation tube.

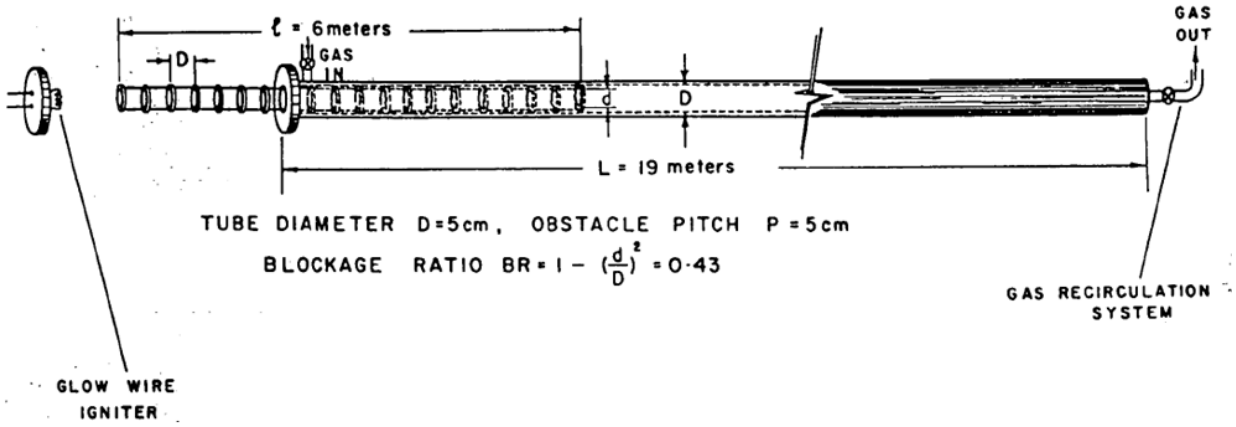

Figure 19: Experimental Configuration Used by Lee for H2-Air DDT Studies Using Orifice Plates with a Blockage Ratio of 43 Percent

B. CFD Model

Due to the symmetry of the orifice plate geometry, an axisymmetric model was used. It was assumed that the axial rods holding the orifice plates had little to no effect on the flame acceleration process and thus could be removed from the CFD model. For the current test case, it was also decided that an unstructured mesh topology would be utilized as shown in Figure 20. The motivation for use of an unstructured mesh was that future analyses would likely involve complex geometries, which make the use of unstructured or hybrid meshes advantageous. Therefore, validation of the Loci/CHEM code's capability of modeling detonation waves and specifically DDT with such meshes was needed.

The unstructured axisymmetric mesh in Figure 20 was generated using the Pointwise software package. A nearly-isotropic mesh with a spacing of 0.254 mm was populated using the advancing front algorithm. Upon review of literature regarding CFD modeling of DDT processes, it was not evident to the author that universal requirements or guidelines existed for mesh resolutions. Rather, mesh resolution requirements appeared to be dependent upon several factors including the chemical mechanism and numerical methods being used. Flame and detonation wave characteristic lengths have been used to help determine the appropriate grid spacing. Potential combustion reference lengths include laminar and turbulent flame thicknesses. Gamezo et al [31] reported the laminar flame thickness to be 0.35 mm for this H2-Air mixture condition. Since the turbulence levels are relatively large for these DDT devices and the Damkohler number (ratio of large-scale turbulent time scale to laminar-flame time scale) is much larger than one, the turbulent flame thickness would be at a minimum, one to two orders of magnitude larger than the laminar flame thickness [30]. Thus, the selected mesh size of 0.254 mm would be more than adequate for resolving a turbulent flame. Another reference

length of interest is the induction length as mentioned previously in this paper. The current spacing corresponds to roughly 0.6 points per the 0.15 mm induction length. Ideally, one should have multiple points per induction length to capture the cellular structure of detonation waves, which are exhibited by the transverse wave mechanism that sustains the detonation front. In previous works [31, 32], a minimum of 100 points per detonation cell width was used to capture DDT events of this nature. For H2-Air, the detonation cell width is roughly 2 orders of magnitude larger than the size of the induction zone. This translates into having approximately 60 points per detonation cell width for the current mesh. Thus, this mesh was determined to be relatively coarse with the potential of being insufficient to capture the DDT. However, one of the key objectives of this work was to fully examine the requirements and sufficiency of the tool for capturing DDT. So while the current mesh was not ideal, it was selected as a starting point to begin examining the test case.

Figure 20 also shows that the boundary layers are not being resolved in the current mesh. The walls were treated as slip walls as the boundary layers were not the primary mechanism for flame acceleration in this system. To simulate the rate of energy release produced by the glow wire igniter, the Loci/CHEM software imposed an energy deposition of 100 W for 1.5 msec into a small zone near the head end of the tube. This provided the equivalent 150 mJ energy release which produced the deflagration in the H2-Air mixture. Lastly, all numerical settings and modeling parameters were the same as those utilized in the previous spherical blast problem including the use of the Shang 7s/7r mechanism.

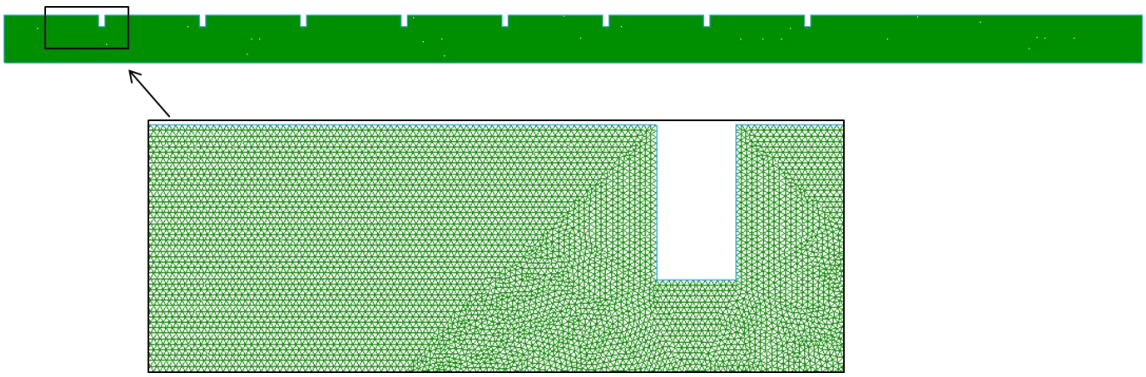

Figure 20: Unstructured Axisymmetric Mesh Used for Orifice Plate DDT Test Case

C. Results

With the selected configuration of a 5 cm tube, blockage ratio of 43% and stoichiometric H2-Air mixture, a DDT event was observed in the experiments to occur promptly near the end of the orifice plates. The obstacle plates prevented the flame from accelerating to a CJ detonation inside the obstacle region due to the flow losses imposed. Rather, complete transition occurred as the flow exited the DDT device as visualized in Figure 21 by Chapin. The transition to a true detonation wave was evident by the increase in flame luminosity that occurs in the fourth image. By the final image, the detonation wave had developed and propagated out of the viewing area.

Figure 22 shows the current CFD predictions at approximately the same points in time as that in Figure 21. Temperature contours are displayed which help visualize the propagation of the flame front. By comparing Figure 22 to Figure 21, it is evident that the CFD analysis was able to reproduce the general behavior observed during the experiments. The ignition of the H2-Air mixture is slightly evident in the first image by a region of elevated temperature. The second

image depicts that the turbulent flame front had propagated to the second orifice plate through the means of a strong vortex ring pattern. Next, the flame front appeared to accelerate to the middle of the orifice plate section and had become highly stretched by the turbulent wakes. The fourth image clearly shows that a localized explosion occurred at the final orifice plate as was observed in the experiments both by Chapin and Lee. The final CFD image depicts the fully developed detonation wave that had formed in the smooth section of the tube. At the detonation wave, a local triple-point was observed due to the presence of transverse waves, which is characteristic of self-propagating detonations [33].

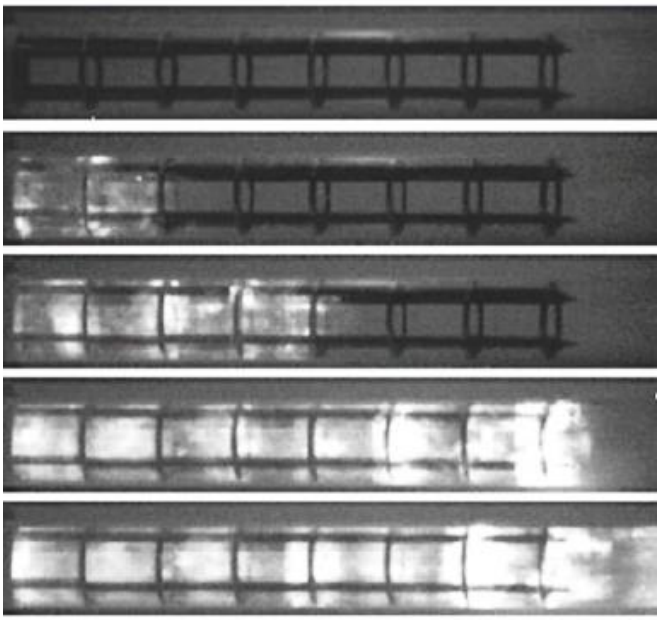

Figure 21: Experimental Visualization of the DDT Process

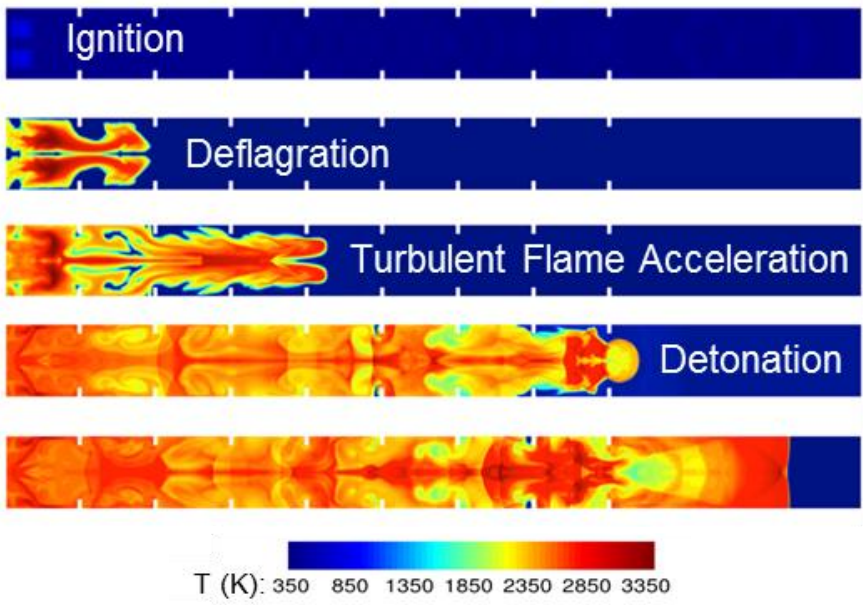

Figure 22: CFD Predictions Corresponding to Experimental Visuals Depicted in Figure 21

Flame speeds and time-of-arrivals were extracted from the CFD results. By nine tube diameters, the flame had accelerated to the isobaric acoustic speed of 1091 m/sec as depicted in Figure 23. It is commonplace for the “onset” of detonation to occur quickly after the flame has accelerated to approximately half the CJ wave speed. This occurred at the end of the orifice plate section (x/D=9.1) as seen by the flame speed being slightly elevated above CJ conditions at x/D=11. By the time the flame front had reached x/D=14, the flame speed had settled to the CJ wave speed.

To better understand the accuracy of the flame acceleration predictions, the time-of-arrival of the simulated flame fronts were compared to that measured by Chapin in Figure 24. For the available data, there was general agreement between the predicted and experimental time-of-arrival magnitudes. However, there were some slight differences in the trends. The experimental data showed almost a linear behavior in time-of-arrival with distance, while the CFD showed a more rapid acceleration from deflagration to the CJ wave speed. This is likely due to modeling assumptions used in the ignition process resulting in a slight offset in the DDT location. The experimental data does not provide sufficient data in the DDT regime near the head end of the tube to capture those effects and thereby provide a more quantitative comparison. However, despite inconsistent ignition conditions, it was demonstrated that the CFD model was capable of predicting the DDT event and acceleration to the correct wave speed.

However, Figure 25 shows a qualitative comparison between the CFD flame fronts and experimental shadowgraphs taken by Kuznetsov et al [34] for a similar configuration. Qualitative agreement is evident between the CFD and experimental flame fronts. A periodically expanding vortex ring appears to dominate the behavior by which the flame front propagates. This flame front became very stretched as the flame continued to flow from one orifice to the next. A small discontinuity in temperature was observed in the CFD analysis along the axis. This was a result of solution degenerations, which characteristically occurs along the axis of an axisymmetric simulation. The real flow does not enforce symmetry, allowing flow to freely cross the axis. The errors induced by the axisymmetric assumption should be resolved by simulating a full 3D geometry. However, despite this small error, the CFD analysis predicted not only the location of detonation wave formation but the general behavior of the flame acceleration dynamics as well. Additionally, these predictions were made with a coarse computational mesh in comparison to previous works. Further study into the sensitivity to mesh resolution was beyond the scope of this preliminary effort. However, the next section will discuss DDT simulations that used even coarser meshes.

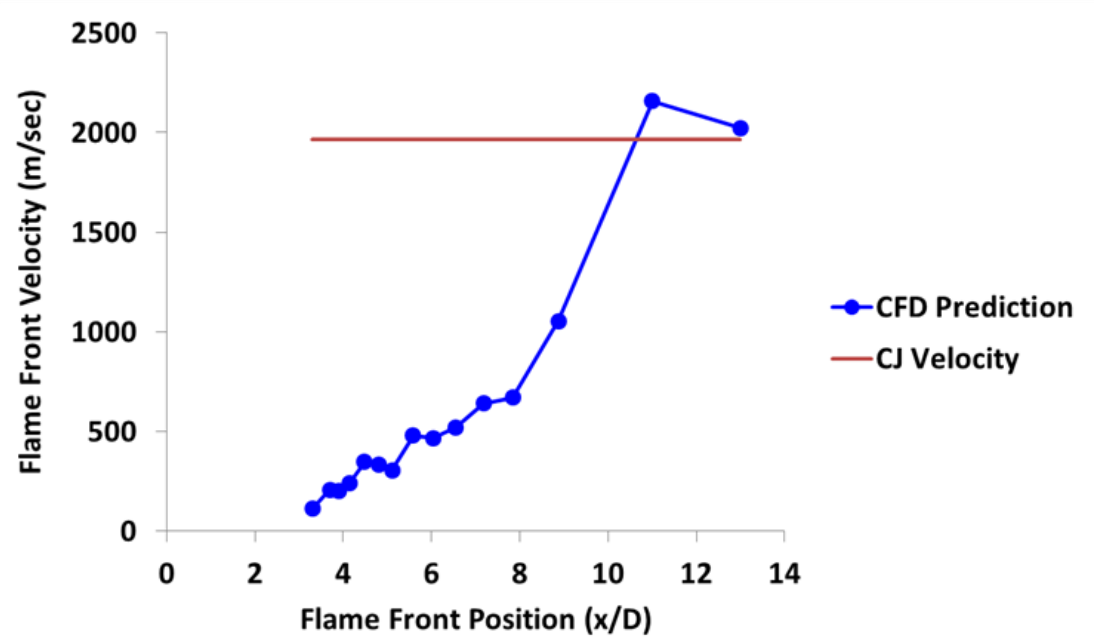

Figure 23: Predicted Flame Acceleration to CJ Conditions

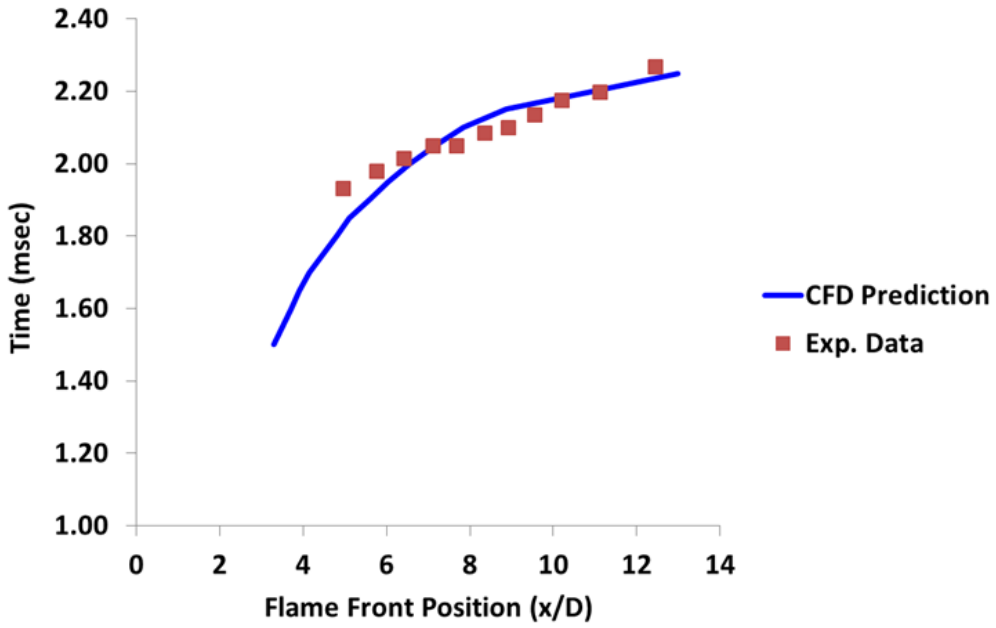

Figure 24: Comparison of Experimental and Predicted Time-of-Arrivals of the Flame Front

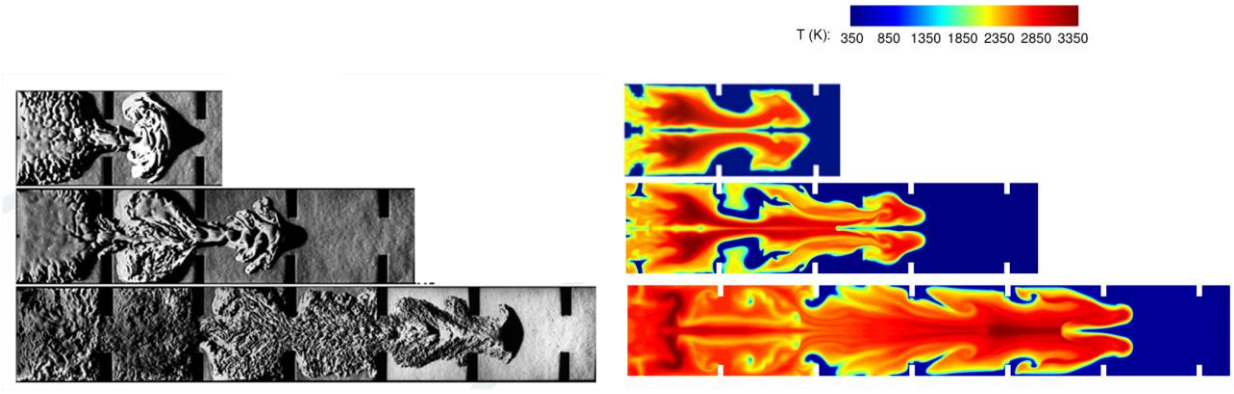

Figure 25: Experimental Shadowgraph and CFD Temperature Field of Flame Acceleration

VIII. Three-Dimensional DDT using a Shchelkin-Type Spiral

A. Background

While orifice plates were successful in generating DDT events for H2-Air mixtures, they suffer from drag losses during the fill, blowdown and purge portions of a pulse detonation engine (PDE) cycle. To improve the efficiency in accelerating DDT, several alternative methods have been developed over the years. One device, commonly referred to as the Shchelkin spiral, is a rod twisted in the shape of a spiral such that it follows the internal surface of the detonation tube as shown in Figure 26. This device, named after K. I. Shchelkin who first introduced it in 1964 [35], has frequently been used in PDE research due to its simplicity and reliability. As such, the Shchelkin-spiral provided a well-defined three-dimensional test case for DDT model validation. It also allowed the use of unstructured meshes on a larger scale to be simulated using the Loci/CHEM code.

Due to the author's familiarity with the ongoing PDE research at the Air Force Research Laboratory, one of their test configurations involving the detonation of stoichiometric H2-Air using a Shchelkin-type spiral was selected. Specifically, the work published by Meyer et al [36] provided a good data set as both high-speed visualizations and pressure measurements were available. The AFRL PDE research was conducted under the leadership of Fred Schauer. The test facility utilized a mechanical valve system constructed from a modified four-cylinder automotive head (Figure 26). The valve system, driven by a variable speed electric motor, provided premixed hydrogen and air to a 2-inch diameter detonation tube. Two of the intake ports served to deliver premixed H2-Air while the other two ports delivered air to "purge" the detonation tube of hot gases after each detonation and before injecting a fresh mixture of reactants. Due to the nature of automotive valving, the division of the cycle timing for various events such as fill-time and purge-time and detonation-time were fixed to be each 1/3 of the cycle. Only one of the four automotive valve sets was used to deliver mass flow to a detonation tube. Several primary operating parameters could be varied during these tests, including equivalence ratio, ignition delay, and fill-fraction. Fill-fraction is the fraction of the detonation tube filled with propellants prior to ignition. In the current test configuration of interest, fill-fraction was one, i.e. completely filled. The premixed hydrogen and air were metered through choked flow orifices. In all tests, the DDT of the premixed H2-Air mixture was enhanced by the use of Shchelkin-type spirals. Typically, the Shchelkin spiral occupied only 10-20% of the total PDE tube length. Dynamic pressure transducers were used to monitor detonation shock speeds and validate that CJ detonations were produced.

Figure 27 depicts the typical cycle of events that occurred during the spiral driven DDT event. These visualizations, reproduced here courtesy of Fred Schauer, were obtained using a transparent polycarbonate tube and a high-speed camera. Initially, a hot spot was visualized downstream of the ignition area due to the threshold setting of the camera. This hot spot continued to grow and propagate along the spiral. Figure 27 shows that localized micro-explosions developed as depicted by the rapid growth in intense flame luminosity. These micro-explosions quickly established forward and reverse-running detonation waves. The reverse-running detonation wave, or "retonation" wave, consumed the remaining propellants towards the head-end of the tube. Once the detonation wave exited the tube, the blow-down process proceeded as indicated by the weakening of flame luminosity. It is this general DDT process that was the focus of the current validation work.

The specific geometry modeled was that used by Meyer et al. A 3/16-inch diameter rod was spun in the shape of a spiral to produce a 1.8-inch pitch (or approximately 1 tube diameter) of 19-inch total length. Premixed stoichiometric H2-Air at standard reference conditions was injected into the tube and ignited at the head-end using a spark plug system. The 2-inch diameter detonation tube was constructed of polycarbonate material so that the flame front could be visualized using a high-speed Phantom camera. A steel pipe combined with high-speed pressure transducers was used to acquire the wave speeds and confirm that a true detonation was established. The overall tube length was 3 feet.

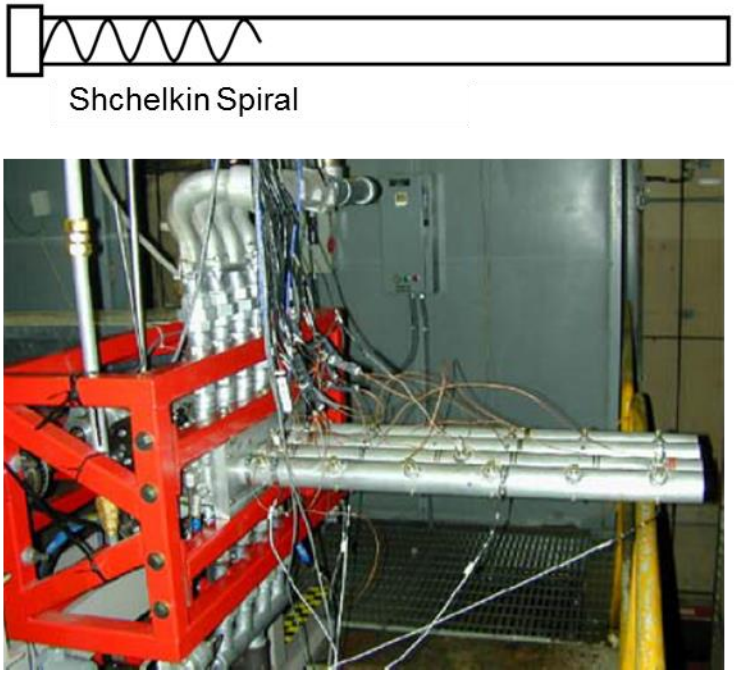

Figure 26: AFRL Experimental Setup of a H2-Air Shchelkin Spiral DDT Tests [Ref. 36]

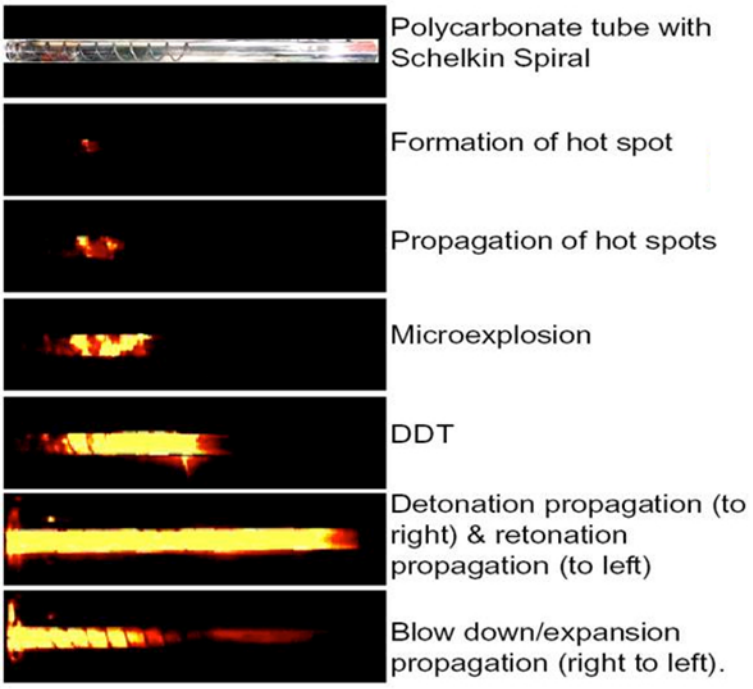

Figure 27: AFRL Visualization of Typical Events during Spiral-Driven DDT Process (Courtesy of F. Schauer, AFRL)

B. CFD Model

The Shchelkin-spiral test case was meshed using the Pointwise software. An initial unstructured mesh of 12.3 million tetrahedral cells was generated using a resolution that was deemed a priori to be the coarsest mesh able to capture the DDT event. This judgment was based on prior experience modeling the propagation of transverse detonation waves in this particular system. In the next section, it will be shown that this model was able to reproduce the DDT event and verify the modeling approach being used. Therefore, a mesh resolution study was not performed as the primary objective of this test case was accomplished with the initial mesh.

Visualizations of the surface mesh for the spiral and head end of the detonation tube are depicted in Figure 28. In addition, a planar cut through the detonation tube has been shown to depict the uniformity in the volume mesh. The average edge length was 1 mm (0.04 inches), which constitutes approximately 1/7 point per induction length. It should be noted that this was the coarsest model used so far in the current work. This coarse resolution corresponds to approximately 15 points per detonation cell-width. While insufficient for fully resolving cellular detonation transverse waves, the mesh was deemed satisfactory for capturing the flame acceleration processes. The surface of the spiral and inner-wall of the detonation tube were meshed with an average mesh spacing of 1 mm as well. This provided approximately 5 points per spiral rod diameter, which is very coarse in terms of trying to resolve wake regions behind the spiral. Again, the purpose of the model was to ascertain the code's ability to qualitatively predict the DDT process at an acceptable level of accuracy for engineering applications.

The boundary layers were not modeled as the walls were treated as inviscid slip walls. The justification for this simplification was that the primary DDT mechanism was believed to be due

to turbulent mixing in the spiral wake combined with local confinement. Lastly, nearly all modeling parameters were the same as that used in the DDT orifice test case except for the time step. Since the three-dimensional spiral mesh was approximately 4 times larger in cell size than that of the two-dimensional orifice mesh, it was necessary to reduce the implicit solver time step to maintain stability with the coarser mesh. It was observed that a fifty percent reduction in time step to a value of 5e-8 seconds was sufficient.

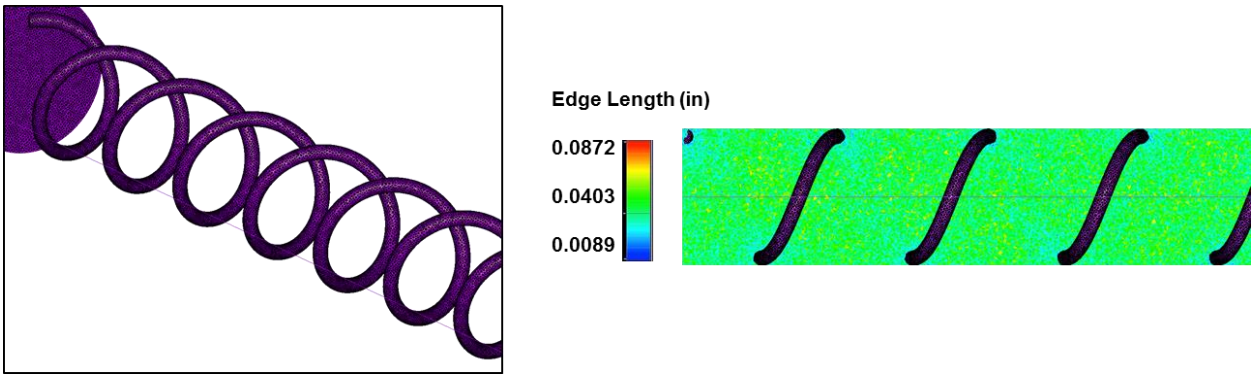

Figure 28: Unstructured Surface Mesh of Shchelkin-Spiral (left) and Center Planar-Cut of Volume Mesh Depicting Uniformity in Edge Length (right)

C. Results

Initialization of the spiral DDT test case was somewhat different than that of previous analyses. During experimental testing, the valve system would inject premixed H2-Air into the detonation tube from the head end. The closing of the valves were timed such that a sufficient amount of H2-Air mixture would be injected to completely fill the detonation tube. Once the valves closed, the spark-ignition would commence providing the energy source for a normal deflagration to initiate at the head-end of the tube. Due to the obstruction produced by the spiral, significant turbulence was generated during the filling process. To mimic this behavior in the CFD analysis, the injection of H2-Air was simulated prior to ignition until steady-state conditions were reached. Figure 29 shows iso-volumes of turbulent kinetic energy being generated in the wake of the spiral. The image clearly shows the helical region of elevated turbulence levels following the path of the spiral. Since turbulence levels control flame acceleration, it is evident that the flame propagation will be highly three-dimensional with increased flame speeds along the spiral. Thus, capturing this initial turbulent flow-field was deemed necessary prior to simulating the ignition process.

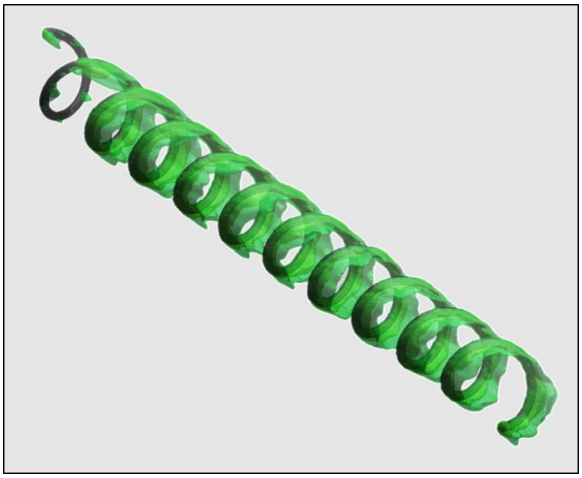

Figure 29: CFD Predictions of the Turbulent Kinetic Energy Generated in the Wake of the Spiral During the Filling Process Just Prior to Ignition

The propellant inflow boundary condition was then switched to a wall to simulate the closed valve condition. At this point, a 150 mJ spark ignition source was provided near the head end of the tube for a duration of 0.1 msec. In the simulations, the H2-Air ignition created a spherical laminar flame that accelerated down the length of the detonation tube. The computed flame speeds were compared to that measured in the experiments as shown in Figure 30. The predicted flame speeds were observed to gradually accelerate until about 4 tube diameters. At this point, the flame acceleration dramatically increased resulting in supersonic CJ flame speeds by 6 tube diameters downstream from the head end of the tube. This behavior closely resembled the empirical curve-fit provided by Meyer et al [36]. Since the CFD model was able to correctly predict both the gradual and rapid regions of flame acceleration, prediction of the location at which self-sustained detonation was achieved.

Figure 31 depicts a side-by-side comparison of the experimental and predicted flame propagations. The experimental flame structure was visualized via broadband luminosity, while visualizing transparent OH density contours ($\rho * Y_{OH}$) approximated the predicted flame structure. Note that globally, the experimental and predicted flame structures follow the same general behavior in time. The first two instances in the time sequence depict a relatively low luminosity flame indicative of a deflagration combustion process. At the third instance in time, local hot spots were generated at the bottom and top of the detonation tubes in both the experiment and simulations. These are localized explosion events, which were the critical pathways for the onset of a full detonation wave. A close-up of the predicted localized explosions has been provided in Figure 32. By the fourth instance in time, the detonation wave was established inside the spiral region. This was consistent with the flame velocity measurements that showed CJ speeds occurring before the end of the 19-inch length spiral (x/D=9.5).

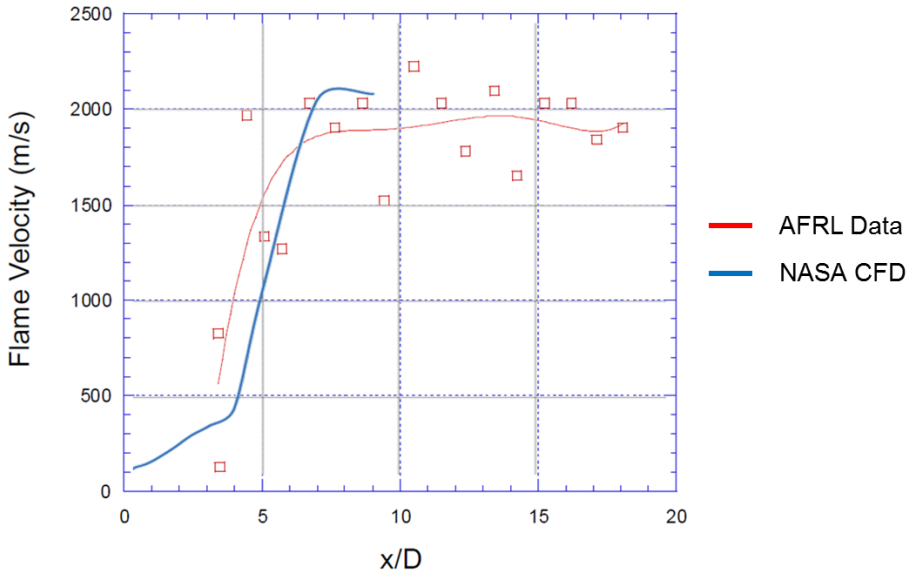

Figure 30: Comparison of Experimental and CFD-Predicted Flame Velocities

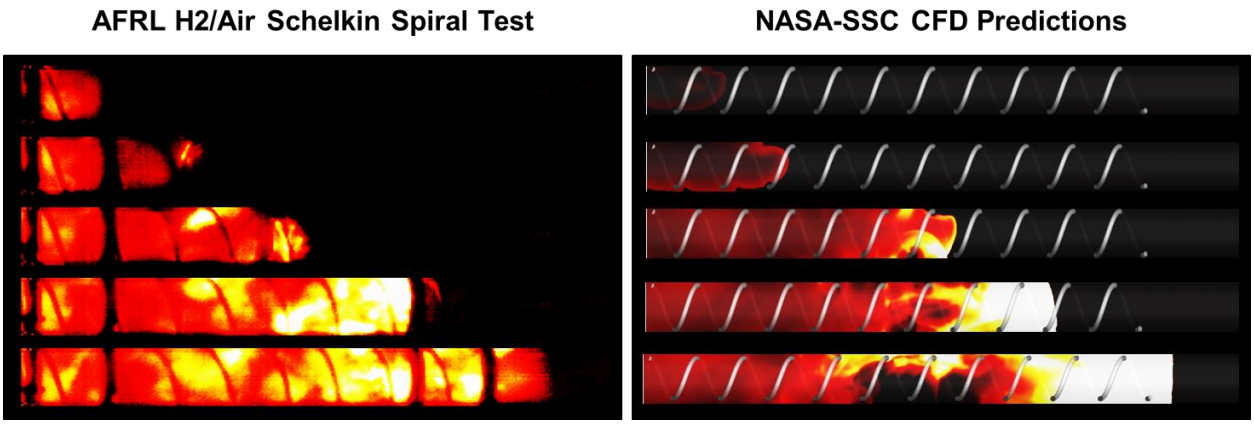

Figure 31: Comparison of Experimental (left) and CFD Predictions of OH Density (right) for the Spiral-Driven DDT Event

Figure 32: Localized Explosion Events Predicted During the Onset of Detonation (Visualized by Center-Plane Cut of $\rho * Y_{OH}$)

It was experimentally observed that the accelerating flame propagated through the spiral region in a non-planar manner. To better visualize the structure of the accelerating deflagration front, high-speed visualizations were taken of the spiral region near the head-end of the detonation tube. Since the detonation was not being visualized, high speed camera was set with increased sensitivity to capture the deflagration luminosity. Figure 33 shows a time sequence of the experimental deflagration wave. The luminous flame was observed to travel along the spiral in a helical path rather than a direct planar propagation down the tube. Figure 34 shows that a similar helical propagation of the flame front was also predicted in the CFD model. In these images, iso-volumes of OH density were rendered and contoured with temperature. This three-dimensional flame propagation is fundamentally different than that produced by the series of orifice plates studied in the previous section. While both the spiral and orifice plates are DDT-enhancing devices that augment turbulent flame acceleration through induced flow separation, the spiral does so with reduced flow blockage. This allows the flame to accelerate to CJ conditions inside the DDT device. An added benefit of the spiral's reduced blockage is lower drag losses, which is critical for detonation-combustion propulsion systems.

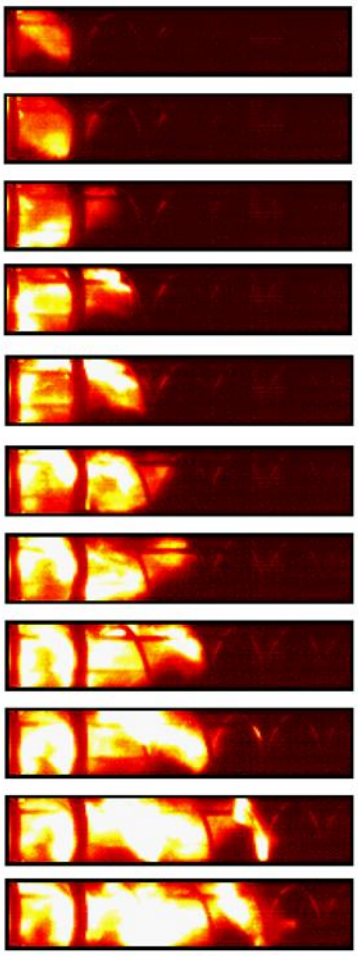

Figure 33: AFRL Visualization of the Helical Propagation of the Flame Front during Deflagration Flame Acceleration

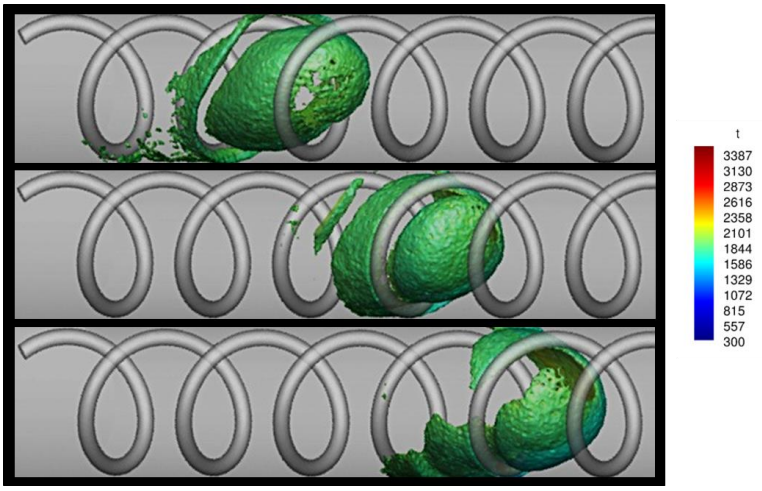

Figure 34: CFD Predictions of the Helical Propagating Flame Front as Visualized by OH Density Iso-volumes (Colored by Temperature in Kelvin)

IX. Flame-Jet Initiation of Deflagration, DDT and Prompt-Detonation

A. Background

In the previous two DDT validation cases, transition to detonation occurred in a confined environment due to detonation tube walls. During rocket engine testing however, the principal scenario in which a DDT event might occur would be in an unconfined or semi-confined environment due to external ignition of a vapor cloud. For example, Figure 34 depicts a typical external ignition of the RS-25 engine during testing at the SSC A-1 test stand. While a detonation did not occur during this event, a substantial overpressure did result from external ignition of a hydrogen vapor cloud, as indicated by the spherical luminous flame surrounding the nozzle exit region. The hydrogen vapor cloud formed outside the rocket nozzle due to the engine's designed operation of leading the flow of hydrogen relative to oxygen during engine start. The excess hydrogen was pushed through the combustion chamber and nozzle but was delayed in combusting due to fuel-rich ignition limits. Retractable H2-Air torch igniters were present on the test stand to propel a turbulent flame-jet into the engine's exhaust and thereby consume the hydrogen vapor cloud as it mixed with the surrounding air. In order to minimize the strength of any overpressure event, the igniters were placed as close to the nozzle exit as possible.

It is certainly feasible under liquid rocket engine testing environments that a scenario might occur in which the hydrogen vapor cloud deflagration accelerates into a detonation should proper conditions exist. Since the majority of our safety devices on the test stands involve small H2-Air torches to burn off excess hydrogen, it was pertinent to investigate the existence of suitable validation data similar cases. Ideally, the validation data set would require conditions in which DDT events did not occur to ensure the model did not erroneously predict a detonation. In addition, since rocket propulsion test applications involve a range of H2-O2-N2 mixtures rather than H2-Air, it was desirable for the data set to consist of H2-O2 propellants with varying amounts of nitrogen.

Figure 34: RS-25 Engine External Ignition at the SSC A-1 Test Stand

Experiments have indicated that detonation initiation using a flame-jet depends on the relative size of the jet (diameter) to the detonation cell-width. Numerous authors have proposed a general linear correlation between jet diameter and cell-width. Figure 35 is a summary chart reproduced from Ref. [37] depicting the relationship between these geometrical and chemical parameters for a H2-O2-N2 system. Open symbols represent test conditions in which the flame failed to transition to detonation, while the closed symbols correspond to conditions in which DDT eventually occurred in the system. In this figure, the relationship of 14 times cell-width and 24 times the cell-width were plotted for reference. While, there does not appear to be a consistent linear relationship that covers the full range of flame-jet diameters tested by these two researchers, the data does suggest a rough order-of-magnitude criterion of $d/\lambda > 24$ might be used with caution for engineering-design purposes.

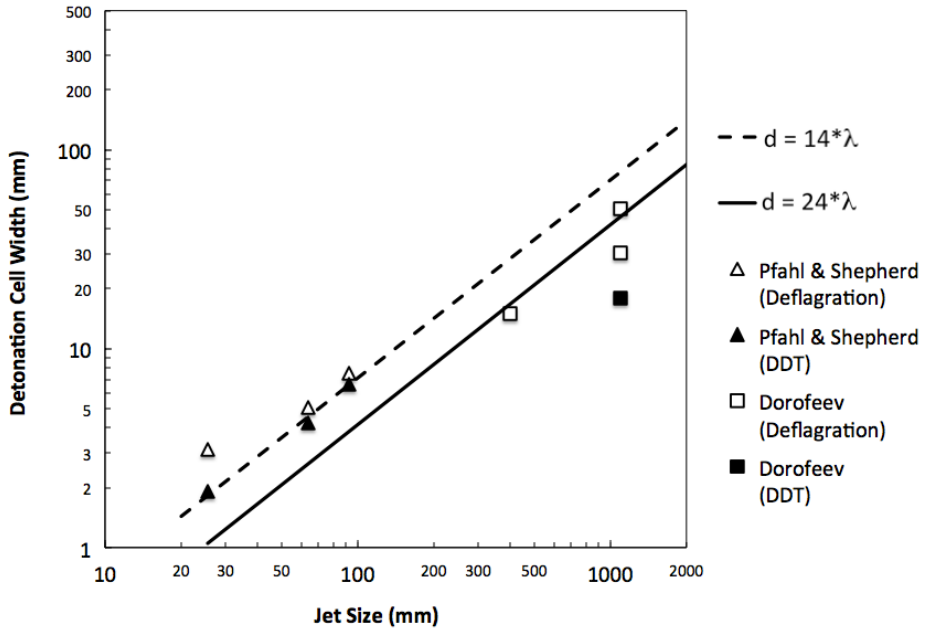

Figure 35: Assumed Linear Correlation for Flame-Jet Initiation of H2-O2-N2 Spherical Detonations

The use of detonation cell-width as a correlation parameter stems from historical roots of fundamental detonation research. Since cell-width is an empirically determined quantity rather than a primary system parameter, its use in the correlation is not intuitive for general engineering applications. Furthermore, cell-width does not really identify the mechanism altering the DDT event as several factors can change the measured cell-width. Some of these factors include equivalence ratio, initial pressure/temperature, and diluent concentrations. For the current application of rocket testing, the primary parameter that would affect the detonation cell-width would be the amount of nitrogen dilution. Specifically, nitrogen dilution alters the acoustic wave speeds and combustion dynamics in such a way that it has a first-order effect on the flame acceleration, DDT and subsequent transverse waves that sustain propagating detonation waves. This sensitivity to nitrogen dilution is thereby exhibited experimentally in the form of changes to the measurable cell-width.

Pfahl and Shepherd conducted their flame-jet initiation experiments in the CALTECH HYJET facility depicted in Figure 36 [38]. This system consisted of a small driver vessel (28 liters) connected to a substantially larger receiver vessel (1180 liters). A diaphragm initially isolated the gas mixtures in the vessels. Inside the driver vessel, deflagration was initiated via spark, which sent combustion gases through a jet nozzle, ruptured the diaphragm, and established a combusting jet flow into the receiver vessel. The experimental facility allowed for adjustments in both the flame-jet size and the mixture conditions in the receiver vessel. Since the volume of the receiver vessel was substantially larger than the flame-jet size, this configuration mimics an “open” environment for DDT to occur. In their study, they proposed a nitrogen/jet-diameter correlation for flame-jet initiation of detonations. Figure 37 shows their data for stoichiometric H2-O2 systems at 1 bar and 295K with various amounts of nitrogen dilution. This is a subset of the same data that was presented earlier in Figure 35, but now provides a more descriptive correlation than that of “cell-width”. The β value in Figure 37, which replaced the cell-width parameter, is the molar fraction of nitrogen to oxygen as indicated by the stoichiometric chemical equation in Figure 37. Using this correlation, the researchers identified three combustion regimes for flame-jet diameters less than 100 mm. The three possible regimes were deflagration, secondary explosion resulting in DDT, and prompt initiation of detonation. For reference, the current author has superimposed a curve representing $D/\lambda \sim 20$ on the figure. While this curve closely matches the prompt initiation/DDT boundary, a linear relationship for the DDT/deflagration boundary does not exist. Since this boundary is more relevant for safety concerns, this data set provides a good source for CFD model validation. The Pfahl and Shepherd data is also well suited for geometrical sizes of interest in rocket propulsion testing, as the exit torches used at SSC are on the order of 2 to 3 inches (25-76 mm) in diameter. The Dorofeev data [39] shown in Figure 35 was also used as validation data for large flame-jet diameter cases.

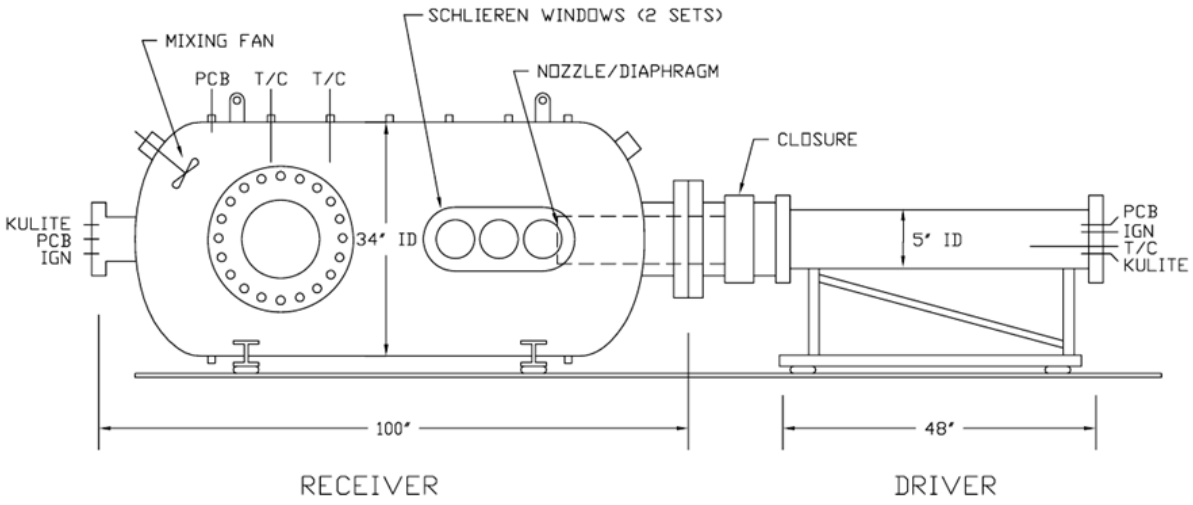

Figure 36: Schematic of the CALTECH HYJET Facility [Ref. 38]

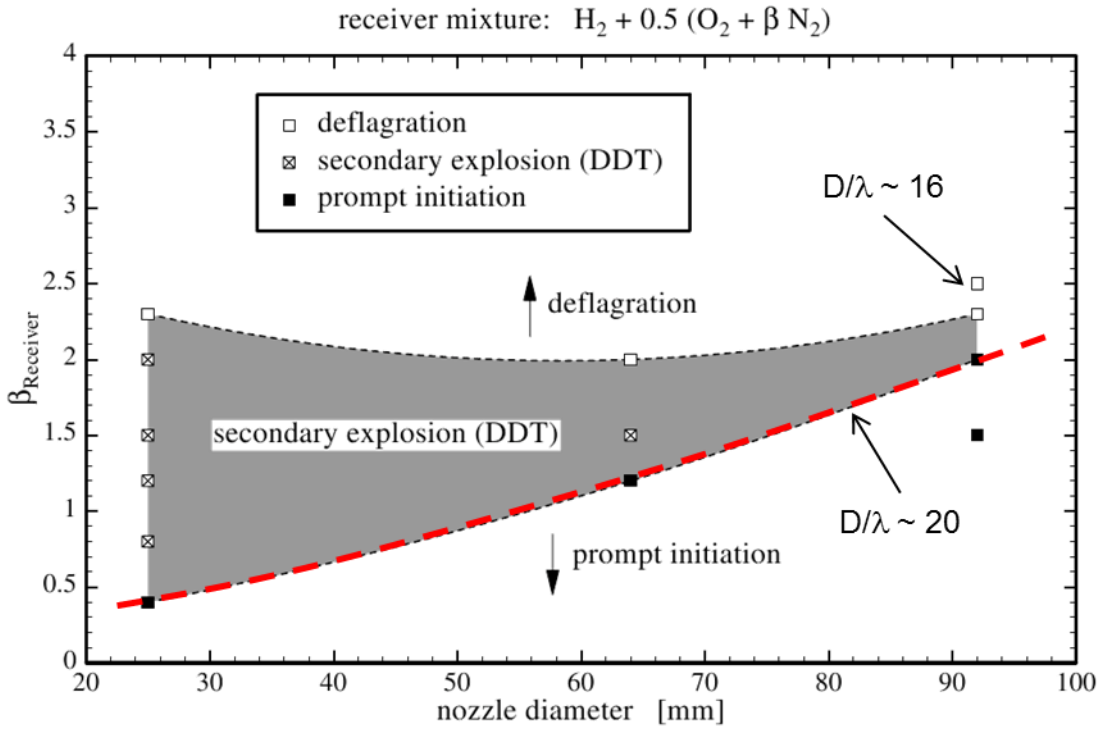

Figure 37: HYJET Facility Data Depicting the Non-Linear Dependency of the Flame-Jet Initiation of H2-O2-N2 Spherical Detonations [Ref. 38]

B. CFD Model

An axisymmetric structured mesh was used to simulate the flame-jet injection into the receiver vessel as depicted in Figure 38. The CFD mesh resolution used in the flame-jet initiation cases was a uniform spacing of 2 mm. Rather than model the entire volume of the

driver and receiver vessels, the driver flow was approximated with a constant mass flow rate of combustion gases as estimated in the experiments. Since the time scales associated with the driver blow-down are much longer than time scales required for establishing the combustion mode in the receiver vessel, the assumption of a constant mass flow inlet was reasonable. Also, the diaphragm rupture, which occurred in the experiments, was mimicked in the CFD model by an instantaneous mass inflow boundary at simulation start. These inflow conditions are summarized in Figure 38. A spark ignition source was not required as the flame-jet provided the means for deflagration initiation in the receiver vessel. The Shang 7s/7r mechanism was used in this study.

A subsection of the receiver vessel was modeled by utilizing supersonic extrapolation conditions for the exit boundaries. The domain size for the receiver region was selected such that the largest flame-jet (Dorofeev, 400 mm) with the longest time to reach a steady combustion state (deflagration, β=3.76) could be fully captured. For the largest flame-jet condition of 400 mm, this corresponded to placing the exit boundaries an axial and radial distance of 10 and 5 jet diameters away from the nozzle exit, respectively. Therefore, smaller jet sizes and/or less nitrogen dilution test cases would have no issue of reaching their final combustion mode within the CFD domain limits. This approach was done to minimize the computational resources required for the study. Lastly, no significant changes were required to the solver settings for modeling the flame-jet initiation cases.

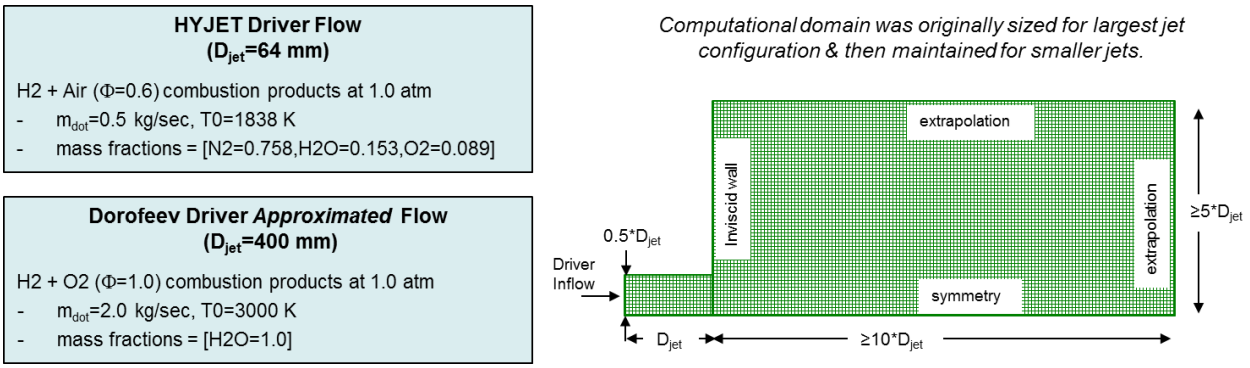

Figure 38: CFD Mesh Topology and Inflow Conditions for Flame-Jet Initiation Studies

C. Results

The smaller jet configuration of 64 mm was modeled with a nitrogen-to-oxygen molar fraction of 1.2. The experimental data of Phafl and Shepherd indicated that this configuration resulted in prompt initiation of detonation within the receiver vessel. Figure 39 provides the predicted density gradients and Mach number contours for this scenario. The CFD results show that the model also predicted prompt initiation as the flame-jet exhausted into the receiver vessel. A hemispherical detonation wave was generated within 5 msec of flow initiation. The Mach number distributions confirm that the combustion is sonic (M=1) relative to the combustion sound speed directly behind the leading shock front.

The simulation was then repeated using the same mesh but with a β=2.0 mixture. This test configuration corresponded to just within the DDT regime of the experimental data set. Figure 40 depicts that DDT was in fact predicted to occur at approximately 10.5 msec after flame-jet injection. This is substantially later in time than the previously modeled test condition with less nitrogen dilution. The DDT in this case was observed to occur on the periphery of the jet as the

flame front expanded. The mechanism for flame acceleration appeared to be due to the well-known Darrieus-Landau (DL) instability exhibited by expanding flame fronts. The DL instability is manifested in the form of corrugated or wrinkled flame fronts due to hydrodynamic instabilities of thin premixed flame fronts undergoing thermal expansion. Along the surface of the flame front, instabilities of relatively small wavelength grow fast causing the “cellular” like deformation with multiple shear-layers being produced in its wake. The flame wrinkling produces local acceleration and under certain circumstances localized explosions in the premixed system.

Simulations of the larger jet diameter case of 400 mm were then conducted. Data was only available from Dorofeev for the case of H2-Air (β=3.76). The simulation results are shown in Figure 41, and they confirm the experimental observation that DDT was not generated under these conditions. Figure 41 also depicts that while the DL instability was present in the expanding flame front, the conditions were such that the flame could not accelerate rapidly enough to produce a detonation. This was not the case when the nitrogen dilution was reduced to β=2.0. By reducing the amount of nitrogen dilution, the DL instability was capable of accelerating the flame to the point in which micro-explosions occurred. Figure 42 shows that at 8.5 msec, density waves had started to accumulate ahead of the flame front. This pressure build-up resulted in continuous acceleration of the flame as indicated by the increasing value in Mach number ahead of the flame front. A localized explosion was eventually produced at 9.5 msec in the jet core. As was seen in the smaller flame-jet of Figure 40, localized explosions also occurred along the flame front well away from the periphery of the jet.

Lastly, the larger jet configuration was simulated with no nitrogen dilution (β=0). These results, provided in Figure 43, confirm the expected prompt-initiation of the detonation wave via the flame-jet. Therefore, while the Dorofeev data does not explicitly delineate the three combustion regimes based on nitrogen dilution, the predicted behavior was consistent with that of the smaller jet data of Phafl and Shepherd.

Two important conclusions can be drawn from the simulation results. First, combustion modes (prompt detonation, DDT, deflagration) were accurately predicted for flame jet initiation of H2-O2 mixtures with varying amounts of nitrogen dilution. This was a critical demonstration that detonation predictions in these environments could be made. However, just as importantly, the modeling approach did not produce erroneous predictions of a detonation when the necessary flame acceleration were not sustainable. The second important conclusion was that the flame-jet initiation models could be conducted with an axisymmetric model. For the cases simulated, it was not necessary to capture three dimensional jet dynamics and their interaction with the flame development. However, this may not be the case for all axisymmetric flame-jets. Also, three-dimensional models would have to be used for non-circular jets, jets with cross-flow or where buoyancy forces begin to play a significant role.

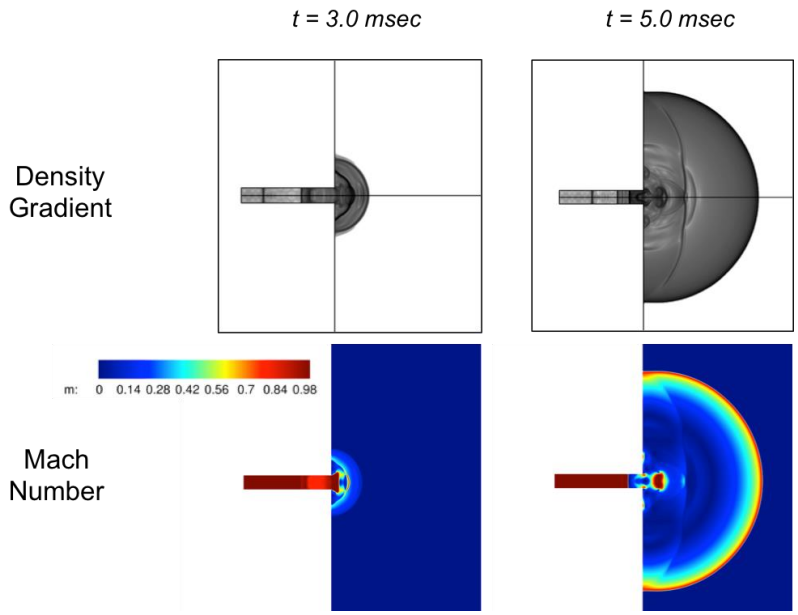

Figure 39: Density Gradient and Mach Number Contours for D=64mm and β=1.2

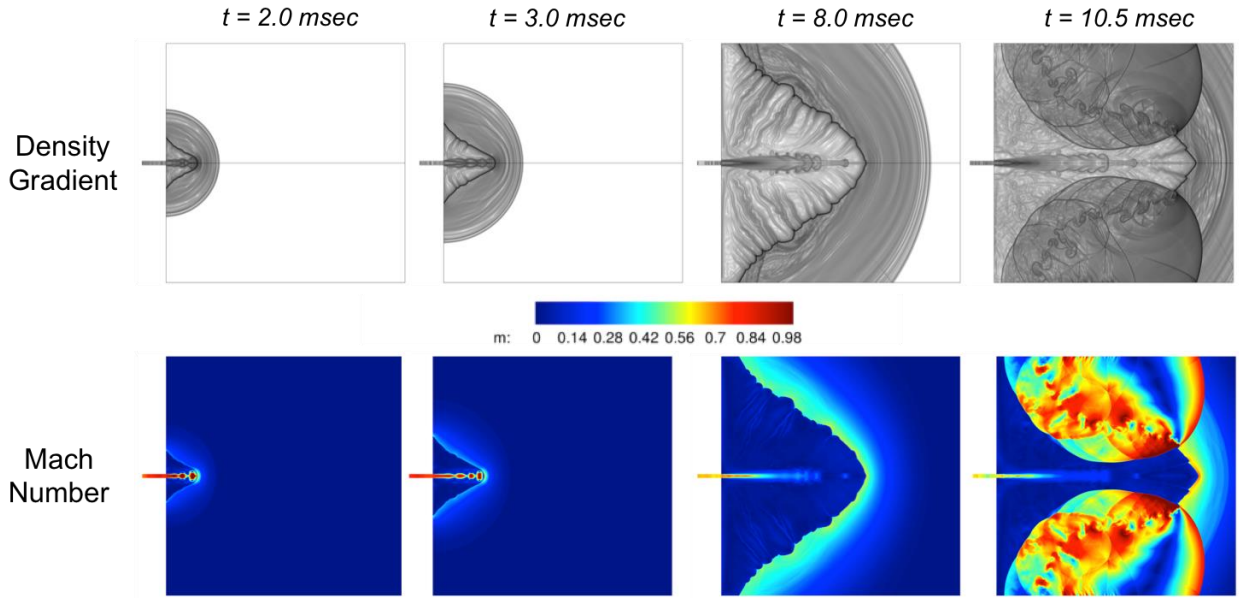

Figure 40: Density Gradient and Mach Number Contours for D=64mm and β=2.0

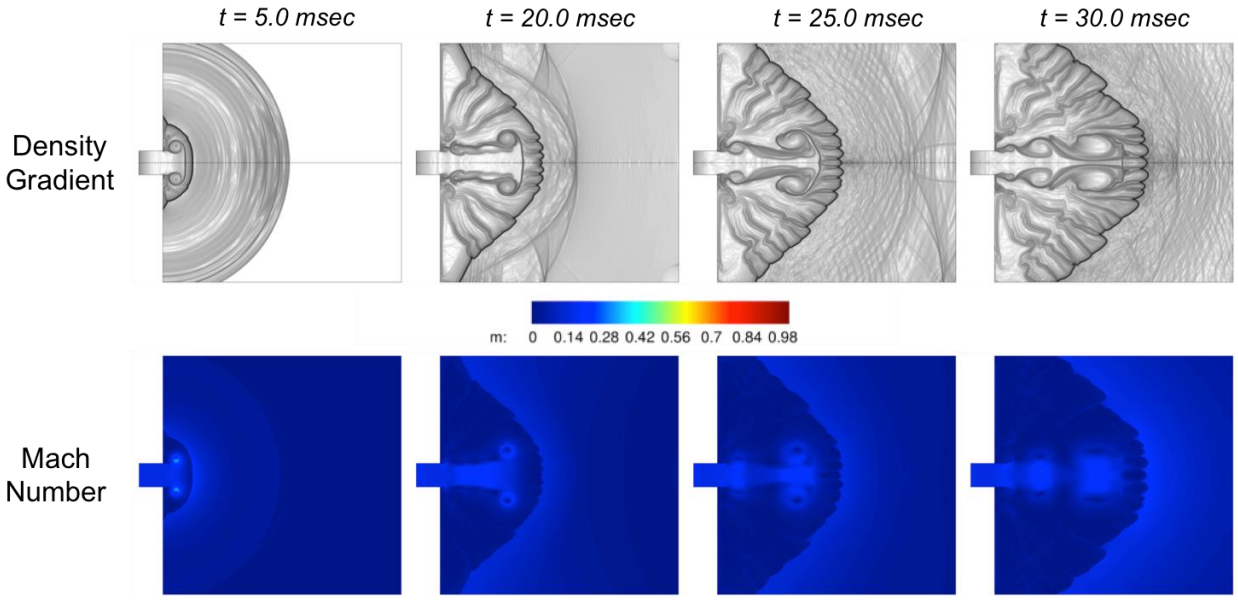

Figure 41: Density Gradient and Mach Number Contours for D=400mm and β=3.76

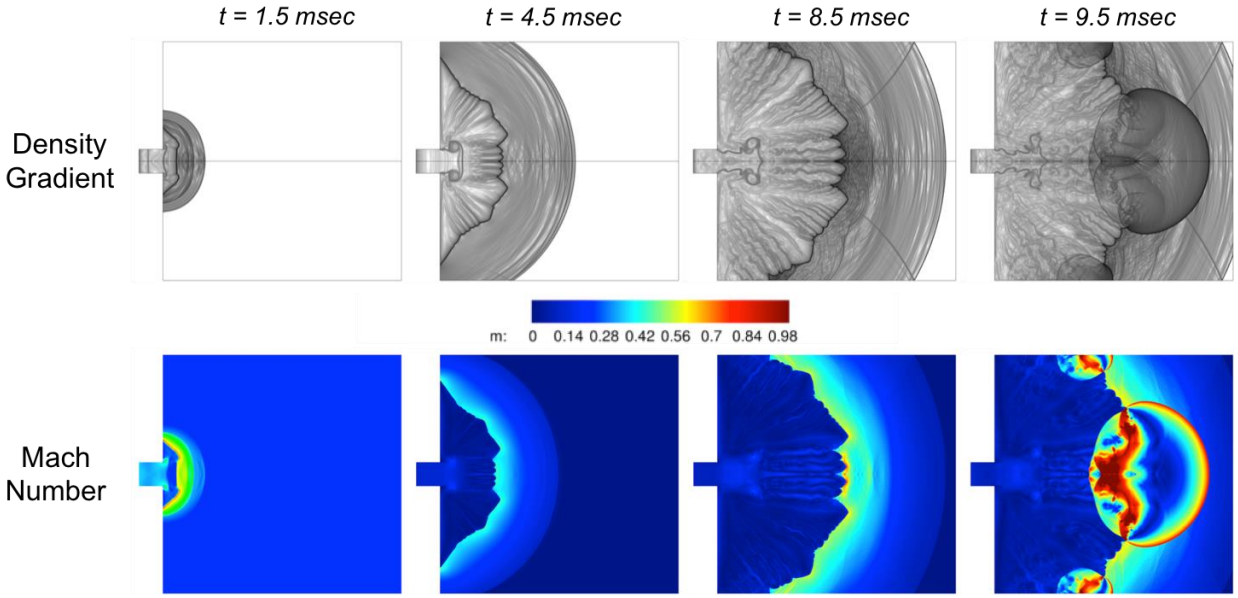

Figure 42: Density Gradient and Mach Number Contours for D=400mm and β=2.0

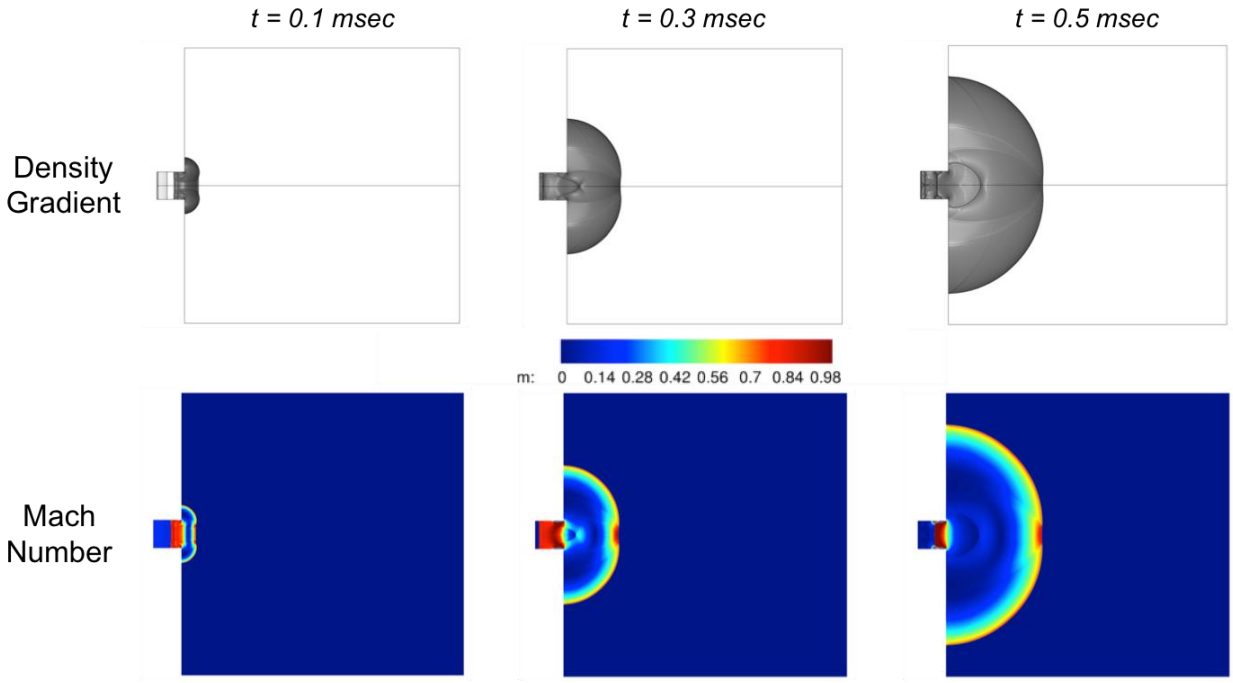

Figure 43: Density Gradient and Mach Number Contours for D=400mm and β=0.0

X. LO2-GH2 Rocket Diffuser Detonation Event at E-3

A. Background

Due to success in modeling fundamental DDT test cases, it was desired that the proposed CFD methodology be applied to a relevant propulsion test problem. Specifically, it was of critical interest to demonstrate the suitability of the technique for predicting both the occurrence of the detonation and any relevant overpressure environments that were generated. Upon review of SSC test programs, a test case was chosen in which a confirmed detonation occurred during simulated altitude testing of a LO2-GH2 subscale engine. The detonation occurred due to delayed ignition. High-speed pressure transducers were available during testing that confirmed a true detonation event had transpired.

Figure 44 shows a schematic of the subscale test configuration in which the detonation was inadvertently generated. The test objective of this program was to conduct subscale verification of potential full-scale passive diffuser concepts, which were to be used during RS-25 engine testing. The subscale test consisted of a small 1klbf thruster with a thrust optimized parabolic nozzle extension designed to approximate the nozzle exit conditions of the RS-25 engine. The exhaust flow from the engine was then fed through a passive rocket diffuser. The rocket diffuser serves to allow the over-expanded nozzle to flow full by “self-pumping” to simulated altitude conditions. Without the rocket diffuser, the flow would separate from the nozzle wall causing excessive side-loads on the engine. To further represent the full-scale test environment, a water-cooled deflector was placed in the diffuser exhaust path, which served to redirect the plume safely away from the test stand. During the test, engine ignition was delayed by 0.3 sec. Due to the magnitude of the propellant flow rates, both the engine and diffuser were completely

filled with H2-O2 at an oxidizer-to-fuel ratio of 5.7. The igniter consisted of a small GO2/GH2 combustion system that injected a flame-jet into the core of the combustion chamber. As was seen in the previous flame-jet initiation studies, DDT was certain when such a situation exists with no nitrogen dilution of the propellants, i.e. β=0. Acceleration of the flame to CJ detonation conditions was verified via high-speed PCB transducers, which were mounted along the diffuser wall. The overpressure environment generated externally to the diffuser was also captured by Kulite pressure transducers that had been placed in the surrounding test area. The intended purpose of these transducers was to obtain near-field acoustic environments for the passive diffuser designs. Figure 45 shows two snapshots of the detonation event. The first picture was taken just prior to engine start and the second picture while the detonation wave was exiting the diffuser.

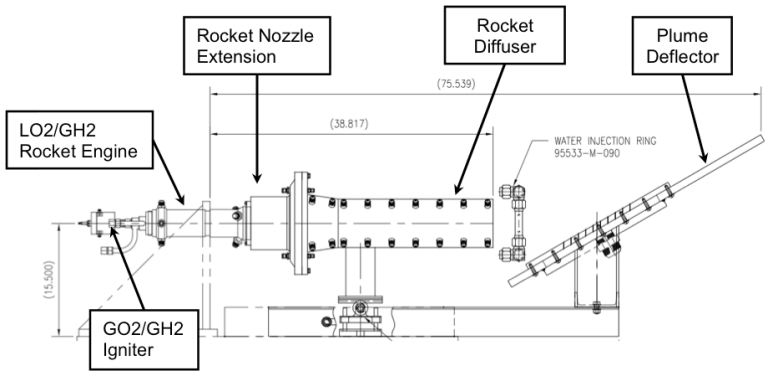

Figure 44: LO2/GH2 Rocket Diffuser Test Configuration at the SSC E-3 Facility

Figure 45: Detonation Event during Altitude Diffuser Testing - (Left) Prior to Start and (Right) Detonation Wave Exiting Diffuser

B. CFD Model

The geometry of the rocket diffuser test configuration was greatly simplified in the current analysis by keeping only the internal structure of the engine and diffuser. The thrust takeout structure, test facility support beams and instrumentation hardware visible in Figure 45 were removed for simplification. Also, the water spray ring and plume deflector located at the exit of the rocket diffuser was removed from the model, as it did not affect the DDT process. Upon implementation of these geometrical and flow-field simplifications, an axisymmetric mesh could

be used. However, one significant impact of these simplifications was that the external overpressure environments were not as accurately modeled because the various surfaces for wave reflections and amplifications were removed. Also, attenuation of the blast wave by the water sprays was not captured in this single-phase flow model.

The simplified axisymmetric mesh used is shown in Figure 46. The mesh consisted of unstructured cells with an average edge length of 2 mm in the engine and diffuser regions. This was an isotropic mesh with no wall boundary layers being modeled. Immediately outside the diffuser, the cell size was maintained at 2 mm. The grid cells were then allowed to transition to a 25.4 mm (1 inch) mesh in the surroundings. The solver settings were identical to the previous flame-jet analyses, as no changes to the modeling approach were deemed necessary. The start-up procedure for the simulation was to allow the unburned propellants to first reach steady-state conditions, thereby filling the rocket diffuser with the detonable mixture. The liquid oxygen was assumed to flash vaporize to gaseous oxygen. The igniter flame-jet was then turned on, and the unsteady flame acceleration was modeled until the system reached steady-state operation.

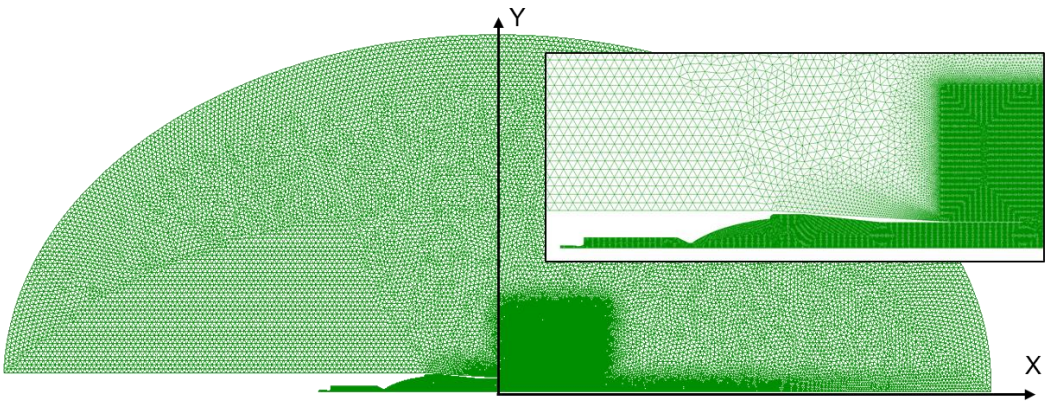

Figure 46: Unstructured Axisymmetric Mesh for LO2-GH2 Rocket Diffuser Test Case

C. Results

The LO2-GH2 rocket diffuser test case was simulated using the Loci/CHEM tool with the Shang 7-species, 7-reaction reduced chemical mechanism. The GO2-GH2 igniter produced a 13.5 mm (0.53 in) diameter flame-jet that was observed to ignite the mixture in the rocket combustion chamber and transition to detonation approximately 47 msec later. The detonation wave is visible in the first density gradient contour provided in Figure 47. This corresponded to 347.8 msec after engine start (t=0). The normal shock in the diverging portion of the nozzle was a result of over-expanded conditions being produced by the flow of unburned propellants through the system. At 347.9 msec, the detonation wave has passed through the nozzle shock and can be seen exiting the engine nozzle in Figure 47. The next sequence of images show the detonation wave passing through the rocket diffuser and exiting into the atmosphere. Due to the “over-filling” of the diffuser with unburned H2-O2, the blast wave continued to propagate along the axis of the exhaust plume of the diffuser at CJ wave speeds, but began to decelerate in the radial direction. This resulted in an oblong shaped blast wave as seen at 348.2 and 348.3 msecs. Due to the lack of propellants outside the radial extent of the diffuser plume, the blast wave decoupled from the flame front. The sequence of images in Figure 48 reveals further shock-flame decoupling as the flame speed decelerated. At approximately 350 msec, the rocket

nozzle started flowing full with combustion gases, and by 353 msec the rocket diffuser had started. The rocket diffuser had started in the sense that the supersonic plume from the engine had fully expanded and attached to the diffuser wall. The rocket diffuser was also flowing nearly full at this time without supersonic flow boundary layer separation. This was consistent with diffuser wall pressure measurements that were taken during the test program. For further validation of the current modeling tool, the predicted steady-state diffuser wall pressure and heat flux distributions were compared to the experimental measurements. Figure 49 shows excellent agreement between the model and experiments for three engine power levels. The engine was operating at the 65% power level condition when the detonation event occurred. Figure 49 shows that the CFD tool was able to predict critical shock reflections and associated increased heat transfer in the diffuser. In addition, flow separation in the diffuser was predicted reasonably well at the reduced power-level of 40%. These results give further credibility to the current modeling approach as a useful tool for modeling supersonic combusting flows associated with H2-O2 rocket propulsion test applications.

The model predictions for the blast environments were also compared to the overpressure data measured during the detonation event. Four pressure-time traces are given in Figure 50. The first measurement was obtained inside the diffuser at the start of the constant-area throat region. A very small time delay of approximately 1 msec existed between the arrival of the measured and predicted waves. However, considering the level of assumptions that had been made in the model, the overall behavior of the pressure-time history was reasonably reproduced. The other three pressure-time traces in Figure 50 were for measurement locations external to the rocket diffuser at the indicated radial and angular positions. These coordinates were relative to the exit of the rocket diffuser where an angular coordinate of zero was in the direction of the exhaust flow. The radial coordinates have been normalized with the diameter of the rocket diffuser. In these three locations, the model was able to capture the peak overpressure fairly well but lacked the fidelity in capturing the secondary pressure oscillations exhibited in the experiments. As mentioned earlier, some lack of fidelity in the pressure-time predictions could be due to the simplifying assumptions regarding the geometry and flow conditions. However, the author believes it could be primarily due to numerical dissipation of transitioning to a 1-inch mesh in the external flow region as this smoothing affect has been observed in the modeling of high-density explosions on rocket test stands [1]. Despite these shortcomings, the model was able to predict the duration of the blast positive pressure, which is critical for estimating loads on surrounding structures. In addition, the time-of-arrival for the blast wave was predicted accurately using the CFD model as shown in Figure 51. Some small error was observed in the early time-of-arrival predictions, which corresponded to the propagation of the detonation wave internally to the rocket diffuser.

These results demonstrate an important outcome of the current study. Namely, the CFD-based modeling approach was capable of predicting a H2-O2 detonation event in a realistic propulsion test environment. The model was able to provide engineering-level accuracy within a reasonable time frame using readily available NASA computational resources. Furthermore, the blast environment peak pressures were predicted using a relatively coarse mesh of 1/14 cell per induction length. This further demonstrates the robustness and practicality of the CFD methodology as an engineering design tool.

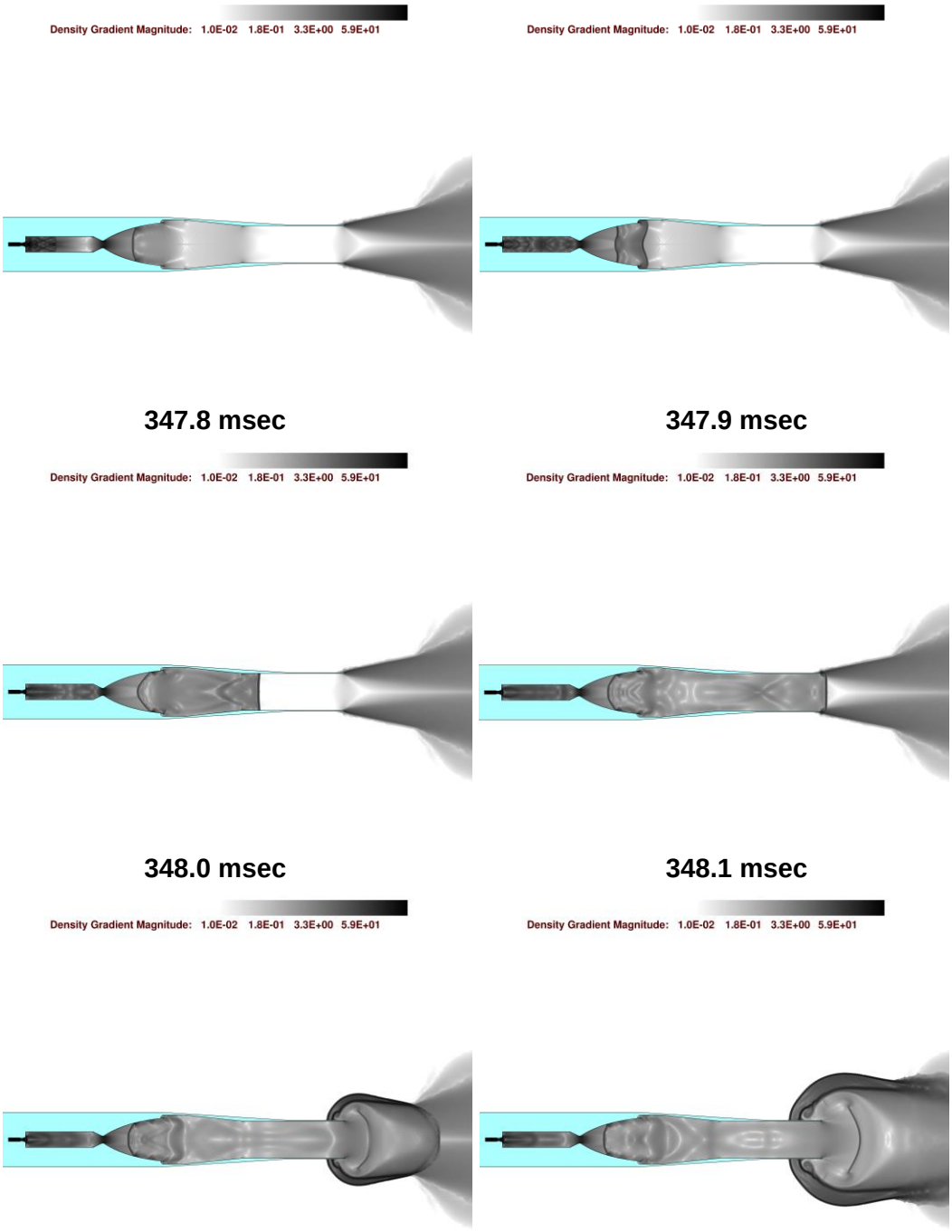

Figure 47: Time Sequence of Density Gradients for Detonation Propagation in the LO2-GH2 Rocket Diffuser

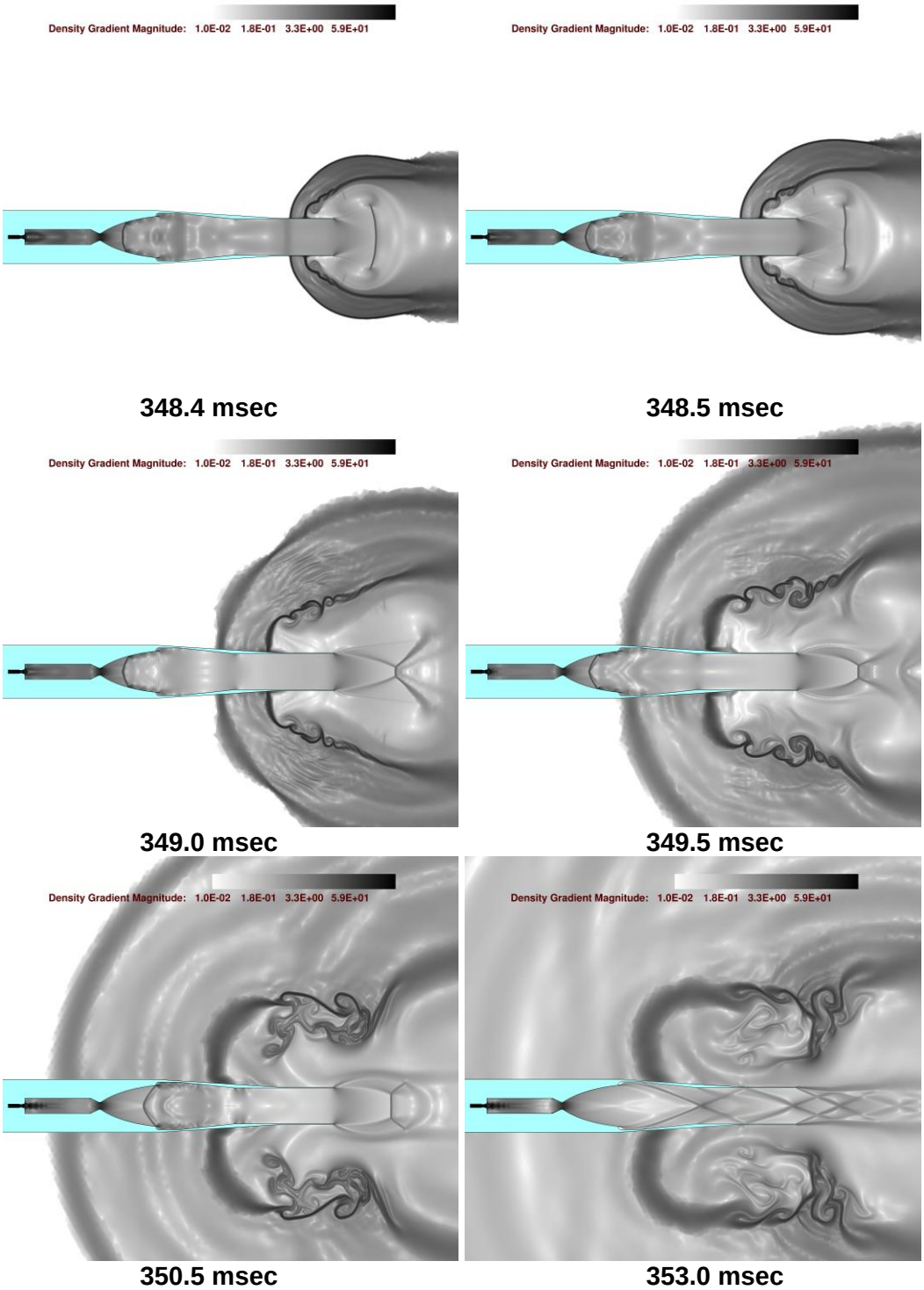

Figure 48: Time Sequence of Density Gradients for Detonation Propagation in the LO2-GH2 Rocket Diffuser (continued)

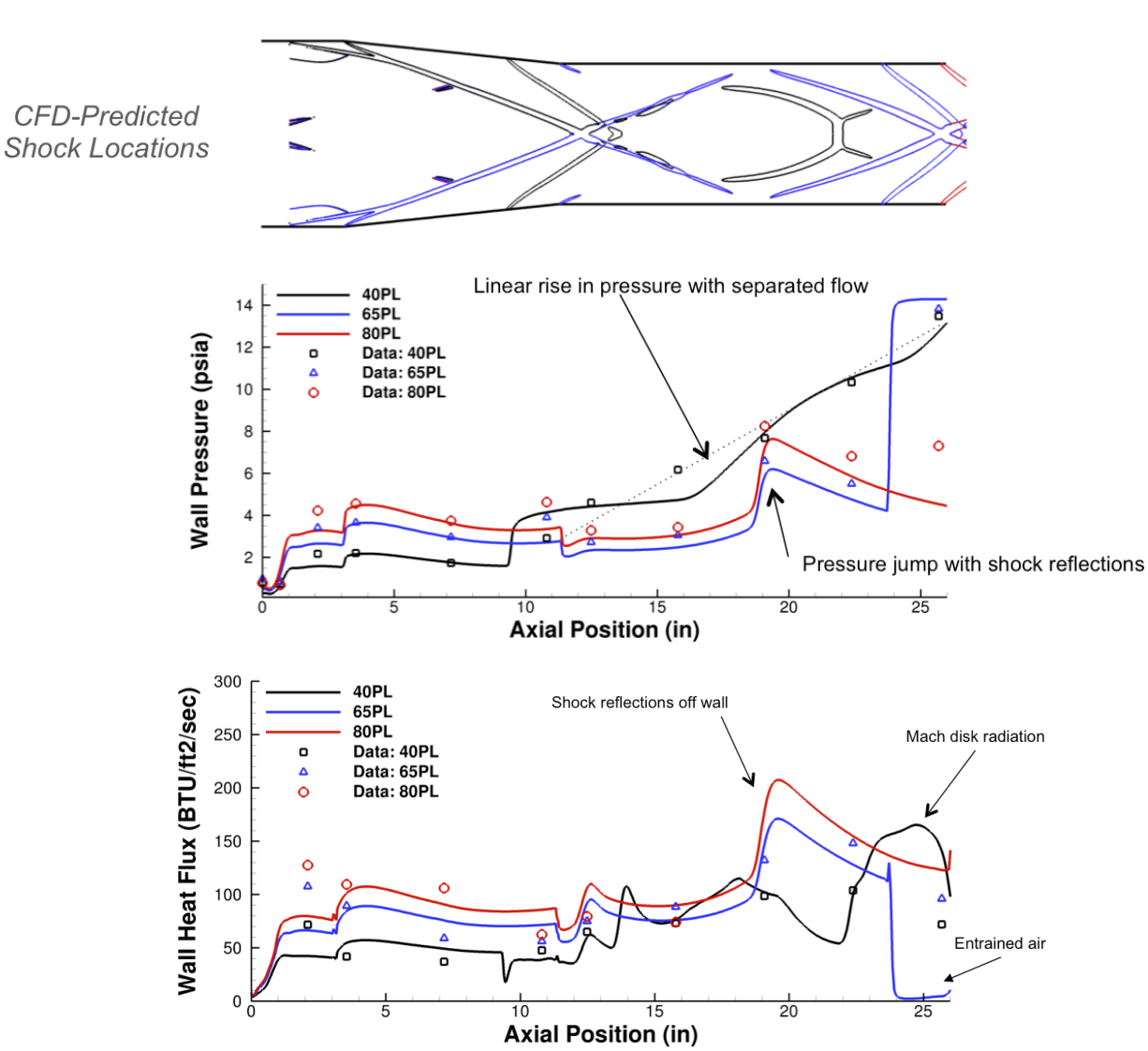

Figure 49: Validation of Steady-State Rocket Diffuser Flow-Field Predictions Shock Structure (Top), Wall Pressure (Middle) and Wall Heat Flux (Bottom) [Color Coded by Power Level: Black 40%, Blue 65% and Red 80%]

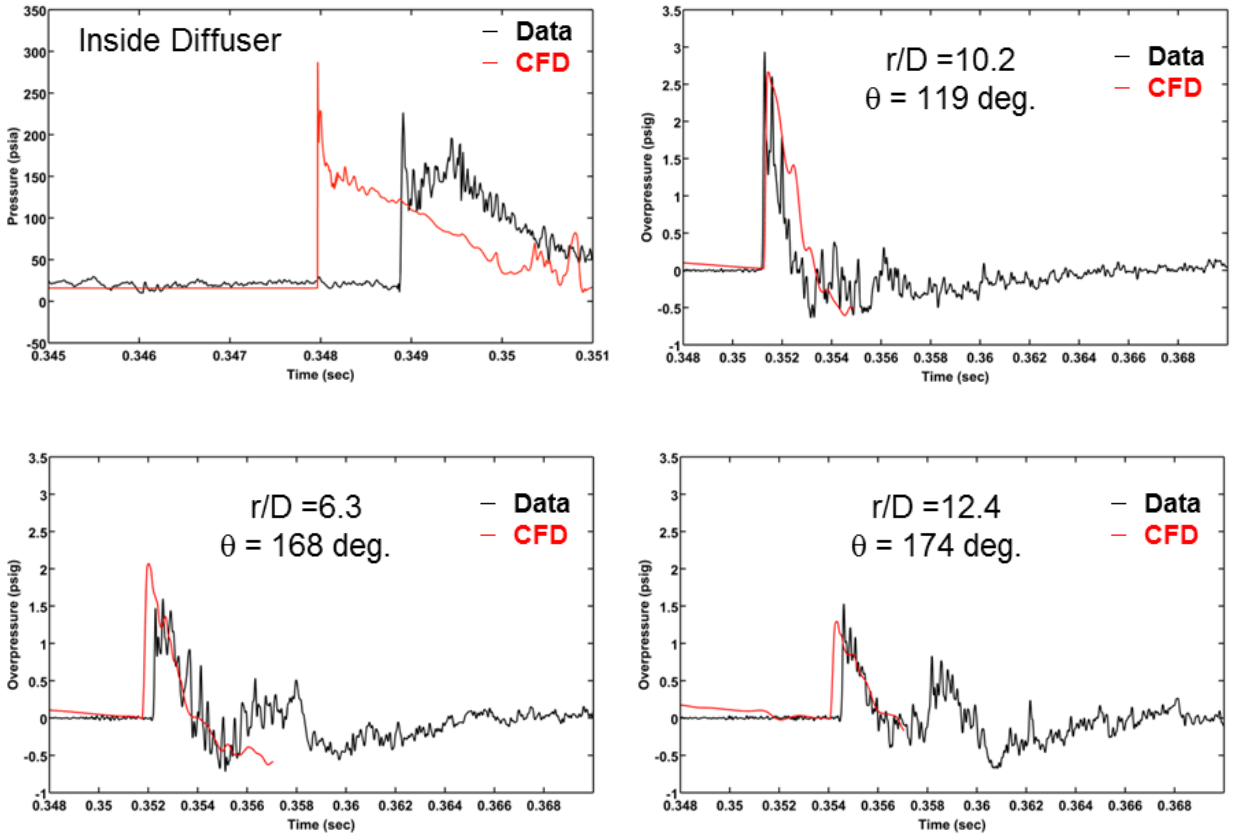

Figure 50: Experimental and CFD Predicted Overpressures

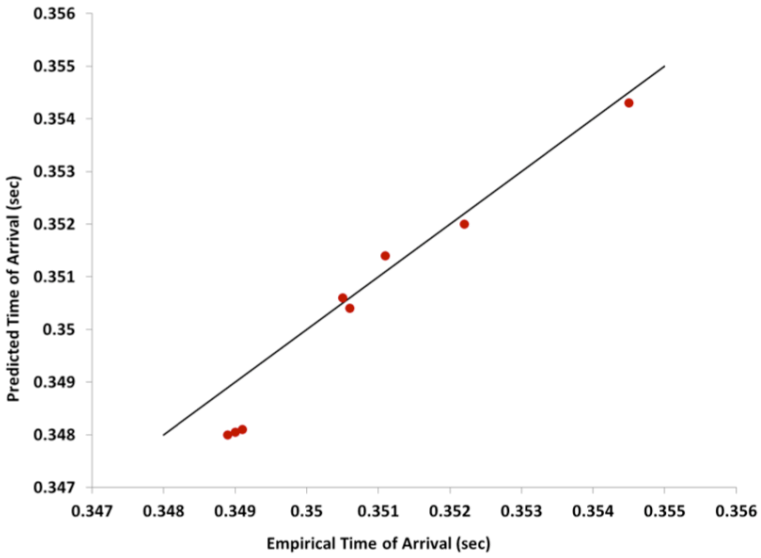

Figure 51: Predicted versus Experimental Time-of-Arrival for the Detonation and External Blast Waves

XI. Summary

A process by which the detonation of H2-O2-N2 mixtures can be reliably modeled using CFD-based methodologies for the purposes of engineering design has been developed. Verification of the Loci/CHEM code with the seven-species, seven-reaction chemical mechanism proposed by Shang et al was completed using CJ theoretical conditions. Validation of the modeling approach in reproducing steady detonation waves was obtained using the Lehr supersonic combustion test case. In these preliminary tasks, the Loci/CHEM tool was observed to provide accurate predictions of the thermodynamics and gas dynamics associated with H2-O2-N2 detonations. Modeling of planar detonation waves inside shock tubes also allowed for the verification of the prediction of non-stoichiometric theoretical conditions. The behavior of unsteady spherical detonation wave dynamics was also examined in relation to standard TNT equivalence approaches used in engineering safety assessments.

After studying basic detonation combustion processes, the efforts of the current work were shifted to more complex processes such as deflagration-to-detonation transition. Test cases were identified for investigating common DDT enhancement devices. For example, the role of orifice plates in flame acceleration was studied. Also, a three-dimensional spiral-driven DDT test case was modeled. In both DDT-enhancement test cases, the models were able to accurately predict the flame acceleration and eventual location of detonation onset with relatively coarse meshes. These test cases also served to demonstrate the robustness of the modeling tool and its suitability for engineering design.

Rocket propulsion testing at SSC frequently involves the combustion of hydrogen vapor clouds through the use of facility torches. These torches are designed to produce high-speed flame-jets that penetrate the vapor cloud that can form near the exhaust nozzle of a rocket engine. To validate the Loci/CHEM tool's capability of predicting both deflagration and detonation modes of combustion in such situations, test cases were selected for study in which relatively small flame-jets were used to initiate combustion in a very large vessel filled with premixed H2-O2-N2. In these test cases, three modes of combustion could be generated: deflagration, DDT or prompt-detonation. The method of controlling the mode of combustion was either changing the jet diameter and/or the amount of nitrogen dilution. The model was observed to accurately predict the dependency of the combustion mode on these parameters. The validation was also completed for flame-jets of similar size to those used on rocket test facilities.

As a preliminary demonstration of the Loci/CHEM tool's capability of modeling relevant rocket test scenarios, a subscale LO2-GH2 rocket engine test case was identified for study. This test case involved passive rocket diffuser testing in which the rocket engine was inadvertently delayed in its ignition resulting in the eventual detonation of the H2-O2-N2 mixture residing inside the engine and diffuser volumes. The model was observed to not only predict this pure H2-O2 flame-jet initiation of detonation, but also reasonably predict the first-order dynamics of the external blast wave. Secondary blast dynamics (reflections, higher-frequency content) observed in the experimental data was not observed in the model predictions. This was attributed to simplifications made to the geometry and flow conditions, as well as numerical dissipation of the relatively coarse mesh in the external flow field. Despite these known issues with the mesh resolution, the CFD-based modeling approach was capable of predicting a H2-O2 detonation event in a realistic propulsion test environment. Also, these predictions were provided in a reasonable time frame using readily available NASA computational resources. The robustness and practicality of the CFD methodology as an engineering design tool was clearly demonstrated.

While significant progress has been made in developing a reliable engineering tool for analyzing detonations relevant to rocket testing, further work is needed in this area. For example, continued application of the modeling approach to actual rocket test configurations is desired. Specifically, further documentation regarding the accuracy of the tool for predicting high-speed deflagrations due to external engine ignition is needed. Also, several rocket launch applications involve the use of small solid rocket motors to propel hot particles into vapor clouds for ignition. The Loci/CHEM code has the capability of modeling solid particles using a Lagrangian-Eulerian framework, and therefore could be used to model such scenarios. In addition to solid particles, the multiphase modeling approach in conjunction with a real-fluid equation of state could be used to model cryogenic liquid detonations. This would be directly relevant to the rupture and possible detonation of propellant tanks and/or piping systems. Lastly, it is of interest to extend the validity of the modeling approach to hydrocarbon detonations. Selection and validation of a proper chemical mechanism for hydrocarbon detonations will enable application of the tool to scenarios involving other common rocket propellants such as methane or RP-1.

XII. References

1 "NASA Engineering and Safety Center 2012 Technical Update", NP-2012-12-445-LaRC, 2012.

2 E. Luke, X-L. Tong, J. Wu, L. Tang, and P. Cinnella, "A Step Towards `Shape Shifting' Algorithms: Reacting Flow Simulations Using Generalized Grids," 39th AIAA Aerospace Sciences Meeting and Exhibit, January 8-11, 2001, Reno, NV, AIAA Paper 2001-0897.

3 Q. Liu, E. Luke, and P. Cinnella, "Coupling Heat Transfer and Fluid Flow Solvers for Multi-Disciplinary Simulations," AIAA Journal of Thermophysics and Heat Transfer, Vol. 19, No. 4, Oct.- Dec. 2005, pp 417-427.

4 Wu, J., Tang, L., Luke, E., Tong, X., and Cinnella, P., "Comprehensive Numerical Study of Jet-Flow Impingement over Flat Plates," AIAA Journal of Spacecraft and Rockets, Vol. 39, No. 3, May-June, 2002.

5 E. Luke, "A Rule-Based Specification System for Computational Fluid Dynamics," Ph.D. Dissertation, Mississippi State University, December, 1999.

6 E. Luke and T. George, "Loci: A Rule-Based Framework for Parallel Multidisciplinary Simulation Synthesis," Journal of Functional Programming, Special Issue on Functional Approaches to High- Performance Parallel Programming, Volume 15, Issue 03, 2005, pp. 477-502, Cambridge University Press.

7 Luke, E., Tong, X., Wu, J., Cinnella, P., and Chamberlain, R., "CHEM 3.3: A Finite-Rate Viscous Chemistry Solver - The User Guide.", January 2013.

8 "NIST-JANAF Thermochemical Tables, 4th edition," Malcolm W. Chase, Jr. Washington, DC: American Chemical Society; New York: American Institute of Physics for the National Institute of Standards and Technology, 1998.

9 Morris, C., and Ruf, J., "Validation of Supersonic Film Cooling Modeling for Liquid Rocket Nozzle Applications," AIAA 2010-6657, 46th AIAA/ASME/SAE/ASEE Joint Propulsion Conference, Nashville, TN, 25-28, July 2010.

10 West, J. S., Strutzenberg, L. L., Putnam, G. C., Liever, P. A., and Williams, B., R., "Development of Modeling Capabilities for Launch Pad Acoustics and Ignition Transient Environment Prediction," AIAA 2012-2094, 18th AIAA/CEAS Aeroacoustics Conference, Colorado Springs, CO, June 04-06 2012.

[11] Menter, F. R., “Two-Equation Eddy-Viscosity Turbulence Models for Engineering Applications,” AIAA Journal, Vol. 32, No. 8, 1994, pp. 1598–1605.
[12] Lehr, H. F., "Experiments on Shock-Induced Combustion," Acta Astronautica, Vol. 17, September 1972, pp. 589-586.
[13] Clutter, J. K., “Computation of High-Speed Reacting Flows,” WL-TR-1997-7059, Contract No. F08635-92-C-0032, July 1997.
[14] Shang, H.M., Chen, Y.S., Liaw, P., Chen, C.P. and Wang, T.S., 1995, "Investigation of Chemical Kinetics Integration Algorithms for Reacting Flows," AIAA Paper 95-0806, 33rd Aerospace Sciences Meeting and Exhibit, Reno, NV, Jan. 1995.
[15] Evans, J. S. and Schexnayder, C. J., "Influence of Chemical Kinetics and Unmixedness on Burning in Supersonic Hydrogen Flames," AIAA *Journal,* Vol. 18, pp. 188-193.
[16] Drummond, J. P, Rogers, R. C. and Hussaini, M.Y.,"A Detailed Numerical Model of a Supersonic Reacting Mixing Layer," AIAA Paper 86-1427.
[17] Ahuja, J. K. and Tiwari, S. N., "Numerical Simulation of Shock-Induced Combustion in a Superdetonative Hydrogen-Air System," AIAA Paper 93-0242, 1993.
[18] Oldenborg, R., Chinitz, W., Friedman, M., Jaffe, R., Jachimowski, C., Rabinowitz, M.and Short, G., "Hypersonic Combustion Kinetics; Status Report of the Rate Constant Committee, NASP High Speed Propulsion Technology Team," NASP TM-1107, NASP Rate Constant Committee, 1990.
[19] Jachimowski, C. J., "An Analytical Study of the Hydrogen-Air Reaction Mechanism with Application to Scramjet Combustion," NASA TP-2791, 1988.
[20] Warnatz, J., "Rate Coefficients in the C/H/O System," *Combustion Chemistry,* edited by WC. Gardiner, Jr., Springer-Verlag, New York, pp. 197-360, 1984.
[21] Yungster, S., and Radhakrishnan, K., “A Fully Implicit Time Accurate Method for Hypersonic Combustion: Application to Shock-Induced Combustion Instability,” NASA TM-10670.
[22] Perkins, H. D., “Effects of Fuel Distribution on Detonation Tube Performance,” NASA/TM-2002-211712, August, 2002.
[23] Barth, T. J. and Jespersen, D. C., “The Design and Application of Upwind Schemes on Unstructured Meshes,” AIAA 89-0366.
[24] Venkatakrishnan, V., “On the accuracy of limiters and convergence to steady state solutions,” AIAA 93-0880.
[25] Quirk, J., “A contribution to the great Riemann debate,” Tech. rep., ICASE Report, 1992.
[26] Einfeldt, B., “On Godunov-type method for gas dynamics,” SIAM Journal on Numerical Analysis, Vol. 25, 1988, pp. 294–318.
[27] Gordon, S. and McBride, B. J., “Computer Program for Calculation of Complex Chemical Equilibrium Compositions and Applications I. Analysis,” NASA RP 1311, Oct 1994.
[28] Lee, J. H. S., Knystautas, R., and Freiman, A., “High Speed Turbulent Deflagrations and Transition to Detonation in H2-Air Mixtures,” Combustion and Flame, Vol. 56, 1984, pp. 227-239.
[29] Chapin, D. M., “A Study of Deflagration to Detonation Transition in a Pulse Detonation Engine,” Thesis, Georgia Institute of Technology, December 2005.
[30] Pope, S. B., “Turbulent Premixed Flames,” Annual Review of Fluid Mechanics, Vol. 19, pp. 237-270, 1987.
[31] Gamezo, V., Ogawa, T., and Oran, E., “Deflagration-to-Detonation Transition in H2-Air Mixtures: Effect of Blockage Ratio,” AIAA Paper 2009-440, 47th AIAA Aerospace Sciences Meeting, Orlando, FL, January 5-8, 2009.
[32] Choi, J. Y., Ma, F. H., and Yang, V., “Some Numerical Issues on Simulation of Detonation Cell Structures,” Combustion, Explosion and Shock Waves, Vol. 44, No. 5, pp. 560-578, 2008.

[33] Lee, J., “Dynamic Parameters of Gaseous Detonations,” Annual Review of Fluid Mechanics, Vol. 16, pp. 311-336, 1984.
[34] Kuznetsov, M., Matsukov, I., Alekseev, V. and Dorofeev, S., "Photographic Study of Unstable Turbulent Flames in Obstructed Channels," *Proceedings of the 17th ICDERS,* Heidelberg, Germany, July 25-30, 1999.
[35] Shchelkin, K. I. and Troshin, Y. K., “Gasdynamics of Combustion,” NASA-TT-F-231, 1964.
[36] Meyer, T. R., Hoke, J. L., Brown, M. S., Gord, J. R. and Schauer, F. R., “Experimental Study of Deflagration-to-Detonation Enhancement Techniques in a H2/Air Pulsed Detonation Engine,” AIAA Paper 2002-3720, July 2002.
[37] Breitung, W., Chan, C., Dorofeev, S., Eder, A., Gelfand, B., Heitsch, M., Klein, R., Malliakos, A., Shepherd, J., Studer, E., Thibault, P., “Flame Acceleration and Deflagration-to-Detonation Transition in Nuclear Safety,” NEA/CSNI/R(2000)7, OECD Nuclear Energy Agency, August 2000.
[38] Pfahl, U. J. and Shepherd, J. E., “Jet Initiation of Deflagration and Detonation in Stoichiometric H2 -O2-N2 Mixtures” Explosion Dynamics Laboratory Report FM99-1, U. S. Nuclear Regulatory Commission Contract NRC-04-94-044, November 2, 1999.
[39] S. B. Dorofeev, V. P. Sidorov, A. E. Dvoinishnikov and A. V. Bezmelnitsyn, Transition to Detonation in Large Confined and Unconfined Fuel-air Clouds, *Proceedings of 15th Int. Colloquium on the Dynamics of Explosions and Reactive Systems*, Boulder, CO, 1995, 421-425.
[40] Kingery, C.N., “Air Blast Parameters Versus Distance For Hemispherical TNT Surface Bursts,” U.S. Army Ballistic Research Laboratory Report No. 1344, Sept. 1966.
[41] NASA-STD 8719.12, “Safety Standard for Explosives, Propellants, and Pyrotechnics”.
[42] Sutherland, L. C., “Scaling Law for Estimating Liquid Propellant Explosive Yields”; Journal of Spacecraft and Rockets; 1978.
[43] D.O.D. Document 4145-21, “Quantity-Distance Storage Criteria for Liquid Propellant,” 1964.
[44] Allgood, D.C., “An Experimental and Computational Study of Pulse Detonation Engines,” PhD Dissertation, University of Cincinnati, 2004.
[45] Strehlow, R. A. and Baker, W. E., “The Characterization and Evaluation of Accidental Explosions,” NASA CR-134779, July 1, 1975.
[46] Sedov, L. I., Similarity and Dimensional Methods in Mechanics, 10th Ed., CRC Press.
[47] Raspet, R., “Shock Waves, Blast Waves and Sonic Booms”, Ch. 27, Handbook of Acoustics, editor M. J. Crocker, J. Wiley & Sons, Inc. New York, 1998.
[48] Jones, J. H., et al., "Acoustic, Overpressure and Unsteady Flow Phenomena Associated with the Saturn Space Shuttle Systems: A Review of Selected Issues", Symposium on Acoustics and Dynamic Environment of Space Transportation Systems, CNES/ONERA, Chatillon, France, Feb. 1994.
[49] Richardson, E., Skinner, T., Blackwood, J., Hays, M., Bangham, M., Jackson, A., “An Experimental Study of Unconfinded Hydrogen/Oxygen and Hydrogen/Air Explosions,” 46th JANNAF Combustion Conference, Albuquerque, NM, 8-11 December, 2014.